Heart Rate Variability in Mice with Coronary Heart Disease

by

Laurence Zapanta

Bachelor of Science
Electrical and Computer Engineering
University of California San Diego, 2002

Submitted to the Department of Electrical Engineering and Computer Science
in partial fulfillment of the requirements for the degree of

Master of Science in Electrical Engineering and Computer Science

at the

MASSACHUSETTS INSTITUTE OF TECHNOLOGY

June 2005

Author . .....
Department of Electrical Engineering and Computer Science
May 19, 2005

Certified by .....
Roger G. Mark
Distinguished Professor of Health Science and Technology
g
or

Accepted by .....
Arthur C. Smith
Chairman, Department Committee on Graduate Students

Heart Rate Variability in Mice with Coronary Heart Disease

by

Laurence Zapanta

Submitted to the Department of Electrical Engineering and Computer Science
on May 19, 2005, in partial fulfillment of the
requirements for the degree of
Master of Science in Electrical Engineering and Computer Science

Abstract

Heart rate variability (HRV), the beat-to-beat fluctuation of the heart rate, is a non-invasive test that measures the autonomic regulation of the heart. Assessment of HRV has been shown to predict the risk of mortality in patients after an acute myocardial infarction. Recently, the Krieger lab at MIT developed genetically engineered double knockout (dKO) mice that develop coronary artery disease accompanied by spontaneous myocardial infarctions and die at a very young age. This thesis investigated whether HRV could function as a prognostic indicator in the dKO mouse.

A novel method for estimating physiological state of the mouse from the electrocardiogram using an innovative activity index was developed in order to compare HRV variables at different times while controlling for physiologic state. Traditional time and frequency domain variables were used to assess the prognostic power of HRV.

Results have shown that none of the HRV variables were helpful in predicting mortality in the dKO mice. Mean heart rate showed some prognostic power, but it was not consistent in all the dKO mice. Finally, the activity index developed in this thesis provided a reliable metric for activity in mice as validated by a camera with motion detection.

Thesis Supervisor: Roger G. Mark
Title: Distinguished Professor of Health Science and Technology
Professor of Electrical Engineering

Acknowledgments

First, I would like to thank Professor Roger Mark, my thesis advisor, for all of your support and guidance throughout the year. Thank you for trusting me and helping me out in a very difficult situation. I am forever in debt.

Thanks to Gari Clifford for supporting me. You provided me with both technical and theoretical insights with my thesis, but you were also there to help and support me as a friend during my most difficult time.

Special thanks to Professor George Verghese for help and advice in classes and life at MIT. You were always available for any problems I encountered.

Thanks to Matt Oefinger for being supportive with my project and making my transition in the lab a lot easier.

I would also like to thank Professor Arthur Smith, Dean Isaac Colbert, Professor David Forney and Marilyn Pierce for guidance and looking out for my best interest.

On the funding side, I want to thank the Information and Communications University in Daejon, Republic of Korea for supporting me for this project.

Thanks to Yu Zhu and Nianya Liu in the Krieger lab for helping setup the camera to monitor the wild beasts.

Thanks to George Moody and Wei Zong for technical input on my project. I also want to thank everybody in the lab for making it a great place to work. Thanks to Tin Kyaw for eating with me at Whitehead.

Finally, I want to thank my family for being there to support me and giving me strength in everything I do, especially my parents. Most of all, I would like to thank Kristen for being patient and supportive all the time especially during stressful times.

Contents

List of Figures

Chapter 1

Introduction

Coronary heart disease (CHD) is a narrowing of the coronary arteries that supply blood and oxygen to the heart. CHD usually results from a build up of fatty material and plaque on the inner lining of the wall of the coronary arteries known as atherosclerosis. There are two kinds of plaques, fibrous and vulnerable. Fibrous plaques have thick walls and small lipid cores which are more stable and cause narrowing, flow limitation and chronic angina. In contrast, vulnerable plaques have thinner walls and large lipid cores. Vulnerable plaques may become unstable and have a tendency to rupture which can partially or completely occlude coronary arteries and lead to ischemia or myocardial infarction (MI), a leading cause of death in the United States. Recently, the Krieger Lab at MIT developed a genetically engineered mouse that models human CHD [3, 6]. These mice die within 8 weeks of age due to severe complications of CHD with extensive MI's. Over the past few decades, heart rate variability (HRV) in humans has emerged as a promising marker of cardiac autonomic tone in varying physiological and pathological states. Researchers have found that depressed HRV after an acute myocardial infarction (AMI) is associated with poor long-term prognosis in humans [2, 7]. This thesis investigates if this relationship is also present in the mouse model.

1.1 Background and Previous Work

1.1.1 The Heart

The heart is in the center of the thoracic cavity suspended by its attachments to the superior and inferior venae cavae and aorta (see Fig.1-1). The heart pumps blood through two separate circulatory systems, one to the lungs and one to the rest of the body. The right side of the heart pump provides the energy necessary to move the blood to the lungs while the left heart provides energy that moves blood through the systemic organs. The following summary of the anatomy and physiology of the heart is taken from Guyton et al. [8].

The pathway of blood flow through the chambers of the heart begins with venous blood returning from the systemic organs to the right atrium via the superior and inferior venae cavae. It passes through the tricuspid valve into the right ventricle and is pumped through the pulmonic valve into the pulmonary circulation via the pulmonary arteries. Oxygenated blood from the lungs flows through pulmonary veins to the left atrium and passes through the mitral valve into the left ventricle. From there it is pumped through the aortic valve into the aorta to the systemic organs. The phase of the cardiac cycle in which the ventricular muscle cells contract is called systole. Diastole is the relaxation portion of the cardiac cycle during which the ventricles refill with blood.

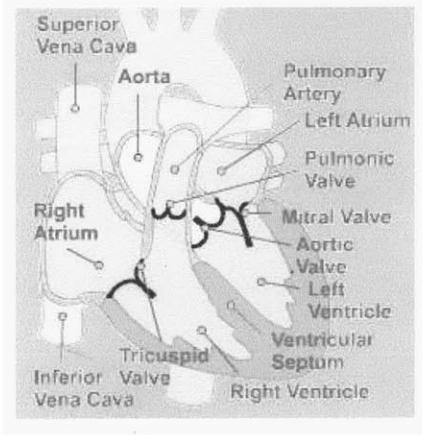

Figure 1-1: Chambers and valves of the heart

The heart is a muscle, which has its own oxygenated blood supply. The coronary arteries supply the heart with blood primarily during the diastolic phase of the cardiac cycle. There are two main coronary arteries, the right and left coronary artery, each with several branches (see Fig.1-2). The left main coronary artery has two major branches: the circumflex branch and the anterior descending branch. These branches feed the lateral and anterior portions of the left ventricle respectively. The right coronary artery and its branches supply blood to the right ventricle, right atrium, the interventricular septum, and inferior wall of the left ventricle. The right coronary artery usually provides the local blood supply to the sinoatrial (SA) node, the atrioventricular (AV) node, and the Bundle of His, which are part of the heart's electrical conduction system.

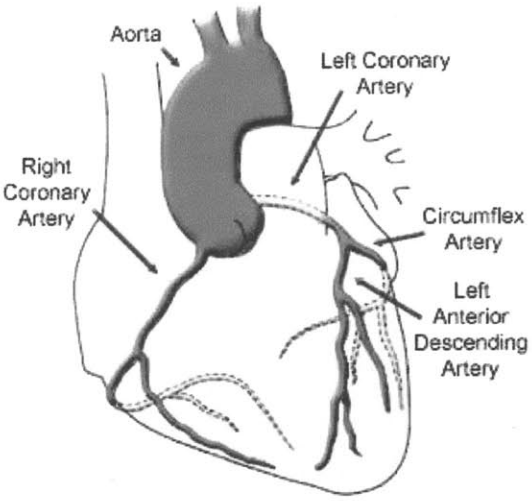

Figure 1-2: Coronary arteries of the heart

The primary function of the heart's electrical conduction system is to coordinate the sequence of atrial and ventricular contraction. It accomplishes this by the conduction of action potentials, which are electrical excitatory impulses, from one cell to the next via gap junctions that link all cells of the heart into a synchronous unit. The components of the electrical conduction system include the SA node, the AV node, the bundle of His, and the right and left bundle branches, which are made up of specialized muscle cells called Purkinje fibers(see Fig.1-3). These muscle cells have

fewer contractile elements and are wider in diameter than other cardiac muscle cells (myocytes) such that they propagate action potentials up to 5 times faster than other myocytes. The SA node functions as the heart's primary pacemaker and initiates the action potentials that are conducted through the heart. The AV node acts to create a slight delay between atrial and ventricular contraction. The Purkinje fibers assure that all ventricular cells contract at nearly the same time.

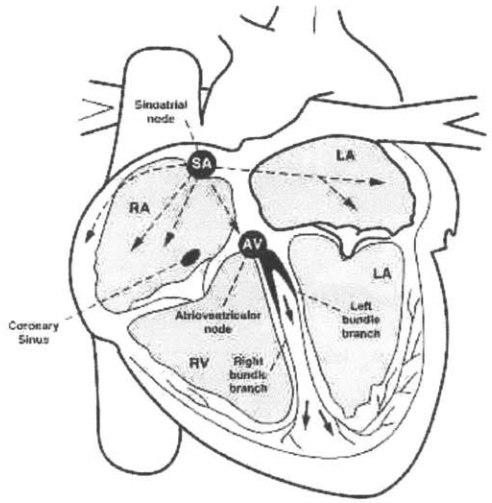

Figure 1-3: Conduction system of the heart showing the sinoatrial (SA) node, atrioventricular (AV) node and the ventricular bundle branches

The intrinsic rate of the SA node is influenced by a balance of inputs from the sympathetic and parasympathetic divisions of the autonomic nervous system. The heart is innervated by sympathetic and parasympathetic (vagus) nerve fibers. The sympathetic nerve distribution is to all parts of the heart including the ventricles. This is in contrast to the vagus nerves which control the parasympathetic stimulation of the heart. The vagus nerves are found mainly in the SA and AV nodes, with a small portion innervating the atria and very little to the ventricles. This anatomic distribution of the sympathetic and parasympathetic nerves to the heart is important to myocardial contractility because the ventricles are responsible for generating most of the force of contraction. When the sympathetic nerves are stimulated, they

release the hormone norepinephrine at the sympathetic nerve endings. This results in an increase in heart rate via the SA node and increased action potential conduction velocity. Because of the presence of sympathetic nerve fibers in the ventricles, an increase in contractility also occurs. Parasympathetic stimulation causes essentially the opposite effects on the heart to those caused by the sympathetic stimulation. Parasympathetic stimulation releases acetylcholine at the vagal endings, which interacts with the cardiac muscle cells. Because the SA and AV nodes have vagus nerve innervation and the ventricles are mostly lacking, the effect of vagal stimulation results primarily in a decrease in heart rate rather than a decrease in contractility of the heart.

Some important measures of cardiac function include cardiac output, stroke volume and ejection fraction. Cardiac output is the amount of blood pumped from each ventricle per minute. It is the product of the stroke volume (the amount of blood ejected per beat) and the number of heart beats per minute. Ejection fraction can indicate the efficiency of myocardial contractility. It is the ratio of the stroke volume to the amount of blood in the left ventricle at the end of relaxation, or left ventricular end-diastolic volume.

1.1.2 The Electrocardiogram

The electrocardiogram (ECG) records the electrical activity of the heart and provides a valuable tool in understanding cardiac activity. The major features of the ECG are the P wave, QRS complex and T wave that are caused by atrial depolarization, ventricular depolarization and ventricular repolarization respectively (see Fig.1-4). The following description of the ECG was adapted from Dubin's textbook [9].

The SA node, the heart's pacemaker, initiates the electrical impulse which spreads outward stimulating both atria. The electrical impulse spreads through the atria yielding a P wave on the ECG. The impulse then reaches the AV node where the velocity of the impulse slows down before it can completely penetrate through the AV node. After penetrating the AV node, the electrical impulse proceeds rapidly down the bundle of His to the left and right bundle branches, and into the Purkinje

fibers which terminate in the myocardial cells of the ventricles. Depolarization of the ventricular muscles causes the QRS complex. The Q wave is the first downward stroke of the QRS complex followed by the upward R wave and ending by a downward S wave. The Q wave is often not present in the QRS complex.

The QRS complex is followed by the ST segment. Normally, no electrical potentials are measured on the body surface during the ST segment. However, myocardial injury or ischemia can produce elevations or depressions of the ST segment. When ventricular cells begin to repolarize, an electrical signal will again appear on the body surface and is measured as the T wave of the ECG.

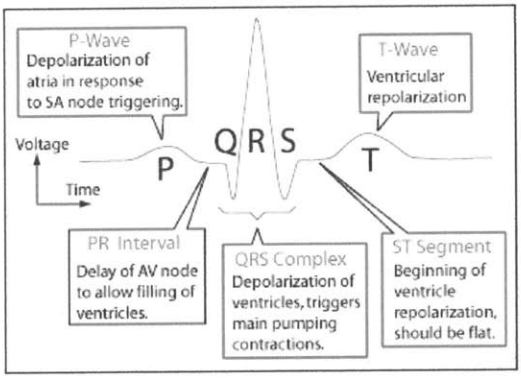

Figure 1-4: Normal electrocardiogram

Automaticity is the property to spontaneously generate an electrical impulse. Cells that have this property can stimulate the heart to beat and are located in the SA node, parts of the atria, AV node and ventricles. The heart is usually paced by the fastest available pacemaker, the SA node that paces about 60 to 100 beats per minute (sinus rhythm). The AV node and the ventricles can pace the heart at a rate of 40 to 60 and 20 to 40 beats per minute respectively.

"If for some reason, a higher pacemaker center fails to generate an impulse, or if the impulse is not properly conducted, a pacemaker lower in the cardiac conduction system will have time to depolarize to its threshold potential and generate an impulse. Such a beat is called an escape beat. A sustained sequence of such beats is called an escape rhythm. On the other hand, if a lower pacemaker site prematurely discharges

because of local increased automaticity, the resultant beat is called an ectopic beat. A series of such beats would thus be an ectopic rhythm [10]".

In a diseased heart, sometimes the electrical signal from the heart's upper to lower chambers is blocked which prevents the passage of electrical stimuli, known as heart block. Heart blocks can occur in the SA node (sinus exit block), AV node or in the larger sections of the ventricular conduction system.

1.1.3 Coronary Heart Disease

The heart provides the force needed to circulate blood to the systemic organs by the coordinated pumping action of its chambers. The orderly sequence of atrial and ventricular contraction is possible only when a healthy electrical conduction system is present. Heart disease such as CHD that disturbs this electrical conduction system can lead to any one of several potentially life threatening dysrhythmias, such as heart blocks. A common cause of heart block is coronary heart disease (CHD) resulting from coronary atherosclerosis.

Atherosclerosis is a disease characterized by a narrowing of the arteries or stenosis caused by a buildup of fatty deposits on the inside wall of the artery. Typically, atherosclerosis consists of lesions confined to the large and middle-sized arteries. Atherosclerosis is heavily linked to hypercholesterolemia with high levels of low-density lipoprotein (LDL) cholesterol as well as low levels of high-density lipoprotein (HDL) cholesterol [3]. When this process occurs in the coronary arteries, CHD develops. The greatest problem with CHD is an imbalance between oxygen supply and demand. When myocardial oxygen demand increases, coronary arteries that are stenosed with lesions are unable to increase blood supply to the heart muscles [11]. This leads to ischemia, a reversible state of inadequate blood flow, which can result in insufficient oxygen delivery to the tissues. Prolonged ischemia leads to tissue death, or necrosis. The ischemic death of the heart muscle or myocardium is known as myocardial infarction (MI) [11].

MI can occur in various regions of the heart wall and may be described as anterior, inferior, posterior or lateral depending on the anatomic location. Twelve lead ECG's

help to localize the affected area through identification of Q waves and changes in ST segments and T waves [9]. The severity of functional impairment after an MI depends on the size of the injury to the heart muscle and the site of the infarction. Acute myocardial infarction (AMI) is usually accompanied by some degree of left ventricular dysfunction, which results in a decreased cardiac output, stroke volume, or ejection fraction [11]. When the left heart is not pumping blood forward, it leads to congestive heart failure and the development of pulmonary edema, which can lead to death.

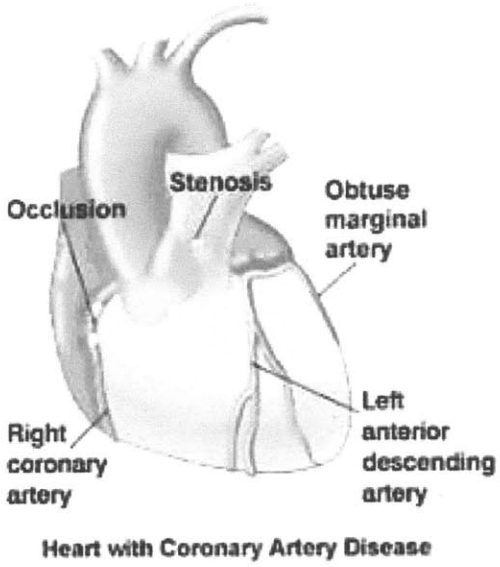

Figure 1-5: Occlusion of the coronary artery

The goal of treatment for myocardial ischemia is to reduce myocardial oxygen consumption or to increase blood supply to the heart muscles. Pharmacologic agents are often employed to manipulate the various determinants of myocardial oxygen consumption, which include blood pressure, heart rate, contractility, and left ventricular volume [11]. The most commonly used classes of drugs are the nitrates, beta-adrenergic blockers, and calcium-channel blockers. For AMI, thrombolytic therapy may be administered. The function of thrombolytic therapy is to activate plasmin, a naturally occurring agent that breaks down the components of blood clots, which

may be obstructing a coronary artery [11]. Other methods of treatment for CHD include mechanical manipulation of stenosed vessels. These include stent placement for dilation of a narrowed coronary artery and bypass grafting where a vein or artery is harvested and used to bypass the existing coronary obstruction [11].

Although CHD is a preventable disease, more than half a million people in the United States die each year from it making it the leading cause of death today. Two Americans suffer a heart attack every minute from CHD, and one of these will die. Lifetime risk of death from CHD after age 40 is 49% for men and 32% for women [11].

1.1.4 Heart Rate Variability

Heart Rate Variability (HRV) is a physiological phenomenon defined as variation in RR intervals (RRI) during normal sinus rhythm. The RRI is defined as the time interval between adjacent QRS complexes resulting from sinus node depolarization (see Fig.1-6). Since the sinus node is subject to both sympathetic and parasympathetic efferent effects, the fluctuations of the RRI have been well accepted to reflect the effects of the autonomic nervous system [12]. The measurement of HRV is non-invasive, often reproducible and rather easy to perform and has led to its popularity as a method for the measurement of autonomic tone in varying physiological and pathological states.

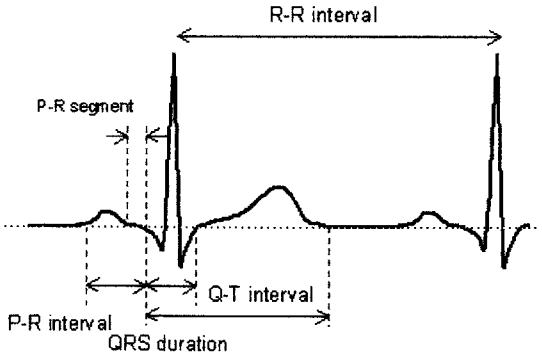

Figure 1-6: Example of the RR interval (RRI). Also shown are P-R and Q-T intervals

Traditional methods of HRV analysis, often referred to as linear methods, include time and frequency domain analysis. Time domain analyses of HRV are usually obtained using simple statistical methods. The simplest time domain parameter is the mean of the RRI (RRmean), which is the average RRI over a given time window. Another parameter commonly used is the standard deviation of the RRI (SDNN) which is sometimes regarded as an estimate of overall HRV.

Other measures include RMSSD, the square root of the mean squared differences of successive NN intervals, NN50, the number of interval differences of successive NN intervals greater than 50 ms, and pNN50, the proportion derived by dividing NN50 by the total number of NN intervals. All these are based on differences between RR intervals and thus are highly correlated, and they all estimate the short-term components of HRV [1].

In 1981, Akselrod et al. introduced power spectral analysis of heart rate fluctuations to quantitatively evaluate beat-to-beat cardiovascular control [12]. Standard methods used for spectral analysis include Fourier transformation (FT) and autoregressive modeling (AR). Investigators usually divide the power spectrum into different spectral bands and calculate the powers in these bands. The spectrum is divided into three or four different bands. The boundaries of the most commonly used frequency bands in humans are as follows:

- ULF - ultra low frequency — < 0.0033 Hz.
- VLF - verylow frequency — 0.0033 Hz - 0.04 Hz.
- LF - low frequency — 0.04 Hz - 0.15 Hz.
- HF - high frequency — 0.15 Hz - 0.4 Hz.

The boundaries have been recommended by Task Force of the European Society of Cardiology and the North American Society of Pacing and Electrophysiology [1].

Understanding of the modulatory effects of neural mechanisms on the sinus node has been enhanced by power spectral analysis of HRV. The motivation for splitting

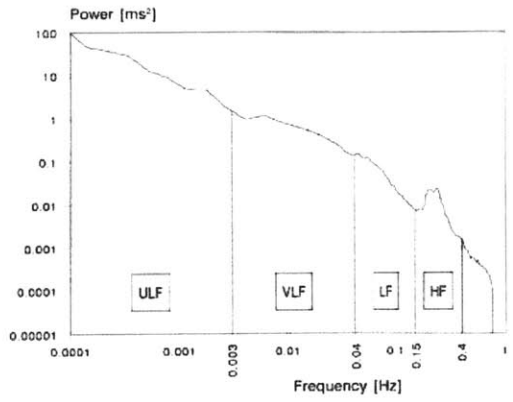

Figure 1-7: Example of an estimate of power spectral density obtained using Fourier Transform. Also shown are the boundaries of the four different bands (Taken from [1]).

the spectrum into different frequency bands lies in the belief that the distinct biological regulatory mechanisms that contribute to HRV act at frequencies that are approximately confined within these bands [13]. The physiological explanation for ULF and VLF bands is not well defined and the existence, if any, of a specific physiological process is still in question. However, it has been well accepted that vagal (parasympathetic) activity is a major contributor to the HF band, as seen in clinical and experimental observations [12]. More controversial is the LF band: although it reflects sympathetic and parasympathetic activity, some consider it as a marker of sympathetic activity only [14]. Since both the sympathetic and parasympathetic nervous system contribute to the modulation of the heart rate, the ratio of power in the LF band to the HF band, known as the $\frac{LF}{HF}$ ratio, is taken as a measure of autonomic balance (also known as sympathovagal balance). Although this measure is widely accepted by investigators, it still remains a topic of much debate [1]. The measurement of the LF and HF power is usually done in absolute power or in normalized units, which represents the relative value of each power component in proportion to the power of the LF and HF components combined.

1.1.5 Heart Rate Variability and Coronary Heart Disease

Coronary heart disease often leads to MI, which can lead to sudden death. Powerful sympathetic reflexes often develop after a massive myocardial infarction primarily due to the inadequate blood flow into the coronary arterial tree [8]. Investigators have been studying changes in HRV indices to assess autonomic activity in patients after MI.

In 1976, using facial immersion, Ryan et al. observed impaired parasympathetic response in patients 3 months after MI. Facial immersion in water 25 degrees C and 0 degrees C provoked less slowing of the heart rate in patients than in age matched controls suggestive of a decreased parasympathetic response in AMI patients [15]. Several years later, reports showed a strong link between depressed HRV and poor long-term prognosis in patients after AMI [16, 2]. In 1983, Wolf et al. found that HRV measured on admission to the coronary care unit in 176 patients with AMI was a predictor of mortality [16]. They found that patients with reduced RRI variability (RRI variance less than 32 ms) in a 60 second ECG recording had a significantly higher mortality rate than patients with a higher RRI variability. In a separate study of 808 patients who survived AMI, mortality was 5.3 times more likely in the group with SDNN less than 50 ms than the group with SDNN greater than 100 ms in a 24 hour recording taken approximately 11 days after AMI [2]. Moreover, in this study, SDNN was also found to be closely correlated to ejection fraction, a measure of the function of the left ventricle which is related to long term prognosis(see Fig.1-8 and 1-9).

Using frequency domain analysis, ULF and VLF power were strongly associated with mortality whereas the LF and HF power were only moderately associated with mortality [17]. The study was done on 715 patients 2 weeks after MI and patients were followed for up to four years. Most studies have focused on HRV between 1 to 2 weeks after MI; however, recent studies have shown that HRV taken earlier is also associated with mortality [7, 18]. Carpeggianni et al. studied 413 patients with new onset of AMI and found that the LF component is an independent prognostic indicator of

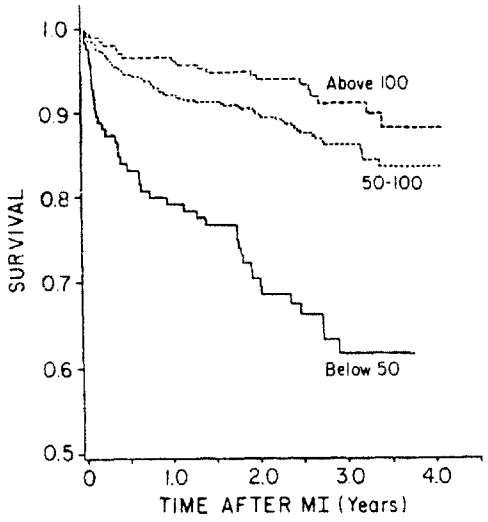

Figure 1-8: Survival vs time after myocardial infarction (MI) in patients with SDNN below 50 ms, 50 -100 ms and above 100 ms (Taken from [2].)

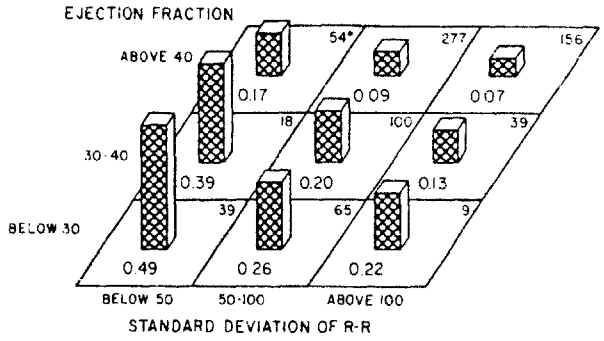

Figure 1-9: SDNN and ejection fraction versus mortality. The number of patients in each group is given in the upper right hand corner. The proportion dying is shown by the height of the bar and the number below each bar(Taken from [2].)

major complications after AMI. The risk of complications increases over 2 fold when the absolute LF power of the RRI series is below 148 ms^2 [7]. Frequency domain measures were obtained from 256 consecutive RRI series and averaged over a 24-hour period to obtain the respective power bands. In another study, using a substudy of the GUSTO (Global Utilization of Streptokinase and TPA for Occluded Arteries) trial, Singh et al., found reduced low frequency to high frequency ratio (LF/HF ratio) was strongly associated with mortality [18]. In this study, HRV measurements were also taken in relation to left ventricular function and patency of the infarcted artery. HRV measures were increased in patients with better ejection fraction (correlated with increased pnn50 and LF component) and angiographic patency (correlated with increased pnn50, LF and HF component).

All of these findings suggest that HRV can potentially be used as a prognostic indicator in CHD. In the last decade, modifications of mouse genome to model human diseases have been rapidly increasing. Recently, a mouse model for human CHD has been developed [3] and will be discussed in the next section.

1.1.6 Mouse Model

Researchers have attempted to create murine models of CHD through genetic manipulation that have the same important features of human disease including hypercholesterolemia, atherosclerosis, lipid-rich coronary lesions, ischemia, MI and cardiac dysfunction. Rodent models that are genetically engineered to have apolipoprotein E (apoE) deficiency, a critical enzyme in the metabolism of LDL, develop severely elevated levels of LDL. Unfortunately, these mice do not usually exhibit the same critical features of human CHD [3].

Recently, the Krieger lab at MIT developed a "double knockout" (dKO) mouse. This mouse has homozygous null mutations in apoE and SR-BI, a scavenger receptor that plays an important role in HDL metabolism [3, 6]. The dKO mice exhibit hypercholesterolemia and dramatically develop atherosclerosis, fibrin-rich coronary artery occlusions, multiple MI's, cardiac dysfunction and most die within 6 weeks of age (see Fig.1-10).

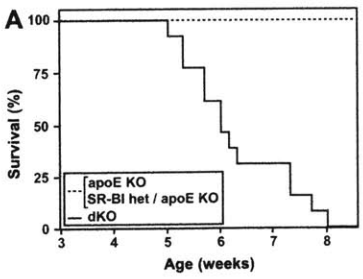

Figure 1-10: Survival percentage of dKO mice as a function of time (solid line). Wild type mouse usually survive about 2 years (Taken from [3]).

The dKO murine model represents human CHD more closely than its predecessor with only the apoE deficiency [3]. Specifically, the dKO mice have enlarged hearts, and extensive MI and scarring. They also demonstrate left ventricular systolic dysfunction, which is indicative of impaired contractility; lower ejection fractions, which measure heart function; and, ECG disturbances such as severe ST depression and dysrhythmias [3]. Angiograms show stenoses and occlusions of the left coronary artery and its branches (see Fig.1-11). Currently, mouse electrocardiograms (ECG) are continuously being monitored and recorded for the purpose of providing a tool to understand and investigate changes in cardiac electrical activity during progression of the coronary artery disease process [5].

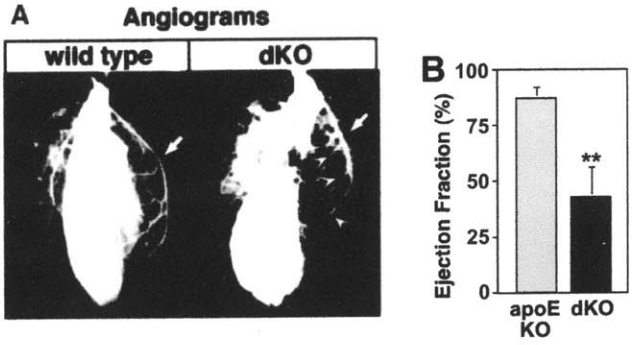

Figure 1-11: Angiograms and MRI based ejection fraction. A) Angiograms of wild type (left) and dKO (right) hearts. The dKO demonstrates multiple stenoses in the left anterior descending artery and its branches. B) MRI based average ejection fractions from apoE KO and dKO mice (Taken from [3]).

1.1.7 Heart Rate Variability in Mice

Lately, there has been an increase in the development of genetically modified mice to model human cardiovascular diseases. Conversely, studies involving HRV to assess autonomic cardiovascular control in wild type and genetically altered mice have been very limited, especially in young mice. Nevertheless, HRV studies have been done in mice using similar human HRV parameters scaled approximately by a factor of 10 to adjust for heart and respiratory rate differences between the two species [4, 19]. In the frequency domain, the regions used for the LF and HF components vary but are concentrated around 0.4 Hz to 1.5 Hz for LF and 1.5 Hz to 4.0 Hz for HF.

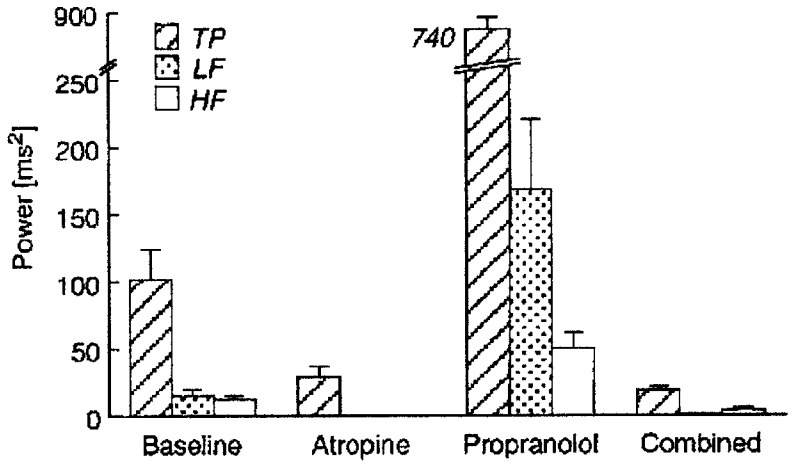

Figure 1-12: Effects of autonomic blockade in frequency domain measures of HRV. Figure taken from [4]

In a study by Gerhmann et al., using these frequency bands, LF and HF power decreased significantly after parasympathetic blockade by atropine [4]. Conversely, sympathetic blockade by propanolol increased both LF and HF components. The study suggested that the HF components were generally modulated by the parasympathetic nervous system, whereas the LF components were influenced by both the sympathetic and parasympathetic system, which implied that LF is not a reliable measure for sympathetic activity (see Fig.1-12). However, scaling of the frequency bands by the approximate ratio of mouse-to-human heart rate was not fully justified.

The effect of the autonomic blockade on the time domain parameters of HRV indicated that sympathetic tone dominates in baseline resting state (baseline heart rate) since atropine had no substantial effect on the RR interval (see Fig.1-13). In addition, the increase in SDNN or overall HRV after sympathetic blockade is possibly due to a saturating effect of the sympathetic nervous system on parasympathetic activity during baseline resting state, which is alleviated after administration of propanolol (i.e. HRV is driven to a more dynamic range) [20].

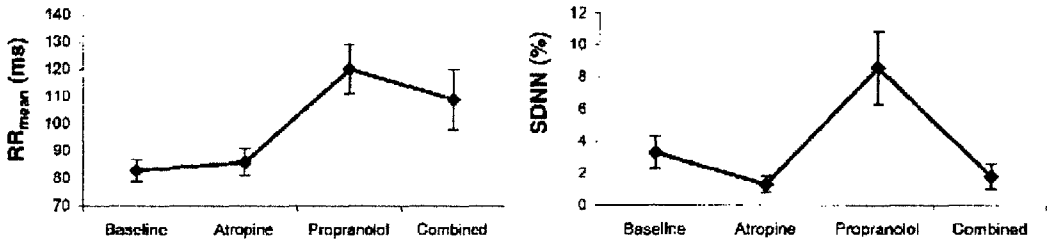

Figure 1-13: Effects of autonomic blockade in time domain measures of HRV. Shown are mean RRI (left) and SDNN (right). Figure taken from [4]

1.2 Goals and Outline

This thesis will analyze HRV in the mouse model of CHD. Specifically, it will investigate if HRV indices in mice have some prognostic value similar to humans with CHD. Mouse ECG is currently being recorded by the Hermes Server (see Fig.1-14)[5]. Preprocessing, extracting RRI as well as HRV analysis will be done using Matlab software. The motivation behind HRV analysis is that it may help biologists track the progression of the disease including monitoring the effects of pharmaceutical interventions.

Before measuring HRV indices, a customized version of the *Pan and Tompkins* QRS detector will be used and developed in Matlab to extract the RR intervals [21]. It is only useful to compare HRV indices in distinct segments when they are taken during a similar or the same physiological state. In humans, physiological states

such as sleep and wake states are commonly recorded and correlated with ECG data. Unfortunately, in the mouse ECG data, physiological state is unknown, therefore, the next step will be to estimate physiological state from the ECG. The most obvious determinants for physiological state from the ECG in mice are heart rate, time of day and physical activity.

An activity index for physical activity is measured in two ways; by measuring the noise content of the ECG and by using the cross-spectral density between the respiratory sinus arrhythmia (RSA) and the ECG derived respiration (EDR) [22, 23]. In addition, it is necessary to make a video monitoring system with motion detection algorithm to confirm the ECG derived activity index. In chapter 2, details of the steps above will be discussed including parameters used for HRV indices. Results of the algorithm and HRV analysis will be presented in chapter 3, conclusion and suggestions for further work in chapter 4.

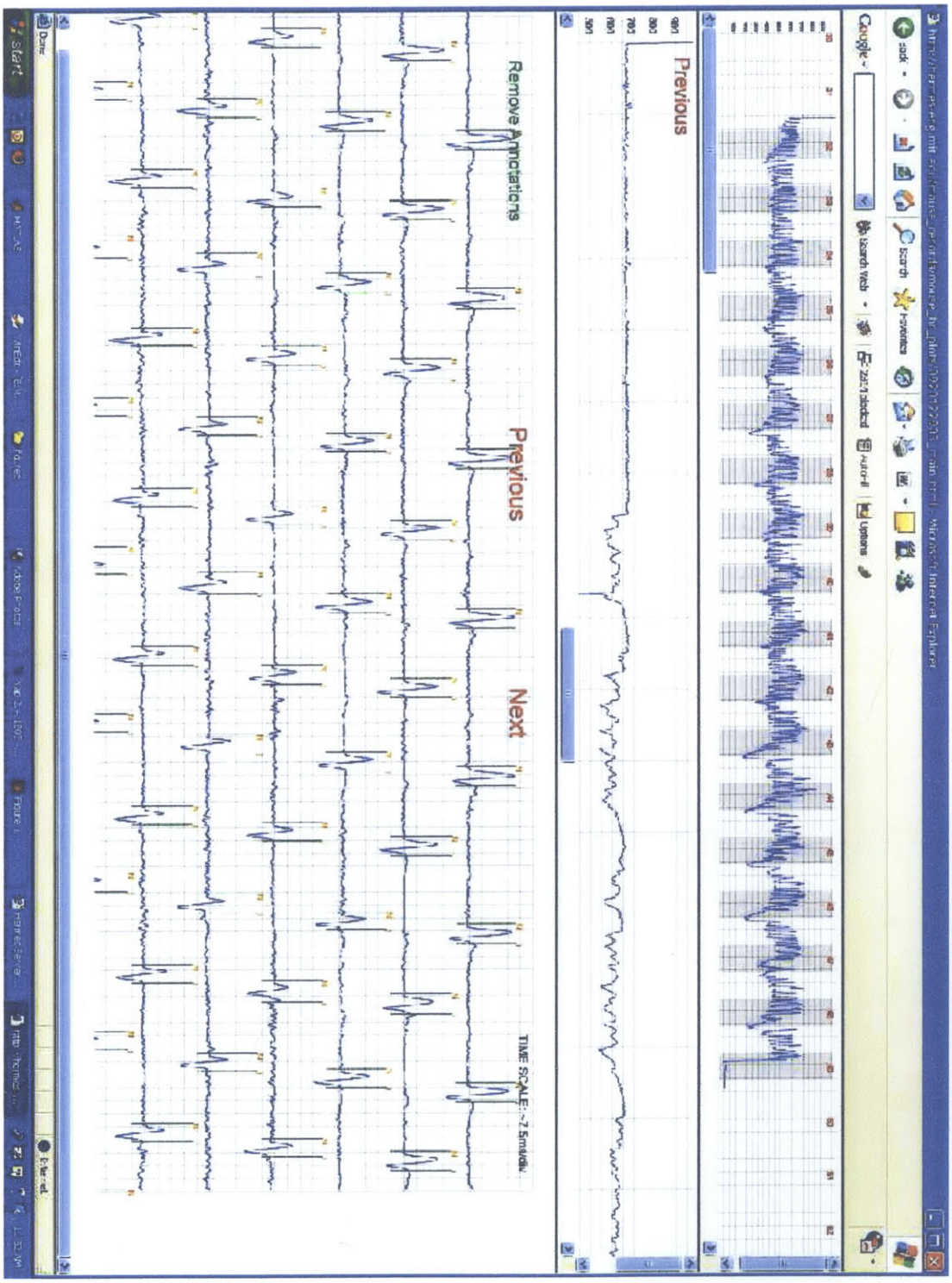

Figure 1-14: Hermes Server (Rotated figure). Figure shows mean heart rate in 10 minute segments (top), instantaneous heart rate in a 10 minute window (middle) and the electrocardiogram (bottom) of a dKO mouse.

Chapter 2

Methods

2.1 Overview

Chapter 1 provided the background and usefulness of HRV indices in humans with CHD. The same standard measures of HRV are applied to the mouse model using mean, standard deviation and power spectral analysis of the RR intervals. This chapter provides a detailed description on how HRV indices are calculated including the extraction of the RR intervals from the ECG. In addition, the method for estimating physiological state using an activity index derived from the ECG is discussed.

2.2 Mouse Electrocardiogram

The mouse ECG is obtained from surgically attached electrodes. Two recording wires are implanted subcutaneously on both sides of the thorax and one is attached on the back as a ground wire. The signal from the electrodes is processed and recorded by the Hermes Server data acquisition system [5]. A simple block diagram below shows the hardware for the data acquisition system (see Fig. 2-1). The system consist of an amplifier, bandpass filter (passband approx. 0.1 - 1000 hz) and an A/D converter. The output of the bandpass filter is sampled at 2 kHz, digitized with 16-bit precision and stored in 10 minute segments [5]. A one second duration of mouse ECG is shown in figure 2-2.

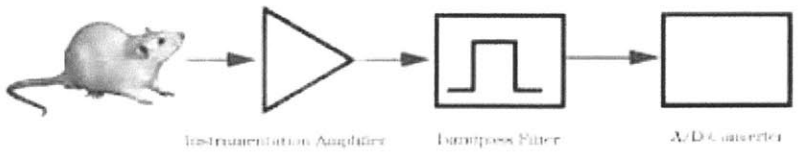

Figure 2-1: Hermes block diagram. Mouse ECG is amplified followed by bandpass filtering and A/D conversion Taken from [5].

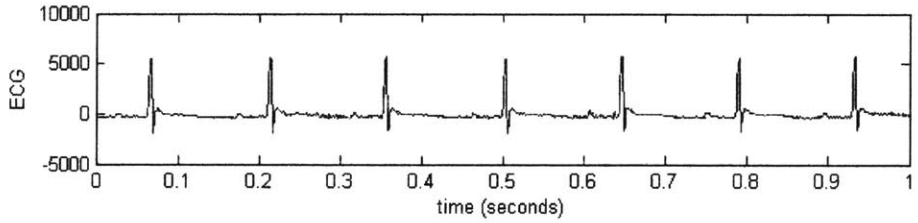

Figure 2-2: Mouse Electrocardiogram.

2.3 QRS Detector

HRV is a measure of the fluctuations in beat-to-beat timing of the heart during normal sinus rhythm. This measure reflects the variation of autonomic inputs into the SA node. Ideally, HRV should be measured using PP intervals which are the time intervals between adjacent P waves. Unfortunately, P waves on the ECG have low signal-to-noise ratios and are very difficult to detect. Most commonly, HRV is measured using RR intervals. The primary reason for this is that the R-peak (QRS complex) is the most prominent feature on the ECG and is easier to detect.

2.3.1 Pan and Tompkins Algorithm

The *Pan and Tompkins* algorithm is used to detect QRS complexes in the mouse ECG [21]. The algorithm consists of two main processes:

1. Pre-processing of ECG signal — this involves both linear and non-linear filtering. The primary function of this process is to filter out ECG noise and help identify regions in which to look for QRS complexes. The filtering processes are

outlined below.

(a) Band-pass filtering (5 - 200 Hz) — a cascade of low pass filter and high pass filter with cutoff frequency 200 Hz and 5 Hz respectively to remove high frequency noise and baseline wander.

(b) Differentiation — differentiation will emphasize the positive and negative slope of the QRS complex.

(c) Squaring — this makes all points positive and does a non-linear amplification of the differentiation output emphasizing the higher frequencies.

(d) Moving-Window Integration — the main purpose of the moving-window integration is to aid in fiducial point localization. In the mouse ECG, this window is about 10 ms wide.

2. Post-processing — this stage decides in which regions of the ECG to look for QRS complexes and extract the RR interval and amplitude of the QRS peak.

   (a) The regions where the fiducial point of the QRS complexes is located when the output of the moving-window integration exceeds a certain threshold. In mice, the threshold is set to 15 % of the maximum moving-window integration output in a one second wide time frame. This threshold is adaptive and changes every one second.

   (b) The fiducial point is then found looking back at the peak of the band-pass filtered ECG within the regions found in the previous step.

The *Pan and Tompkins* algorithm performs very efficiently and correctly detected 99.3 % of the QRS complexes in the MIT-BIH arrhythmia database [21]. The QRS detector seems to work well in mouse ECG. Figure 2-3 illustrates the pre-processing stages of the algorithm and figure 2-4 shows the output (heart rate) of the *Pan and Tompkins* QRS detector compared to the *wqrs* algorithm [24] on a very noisy segment of the mouse ECG. Observe that the beat-to-beat heart rate using *wqrs* algorithm shows more noise artifacts compared to the *Pan and Tompkins* algortihm.

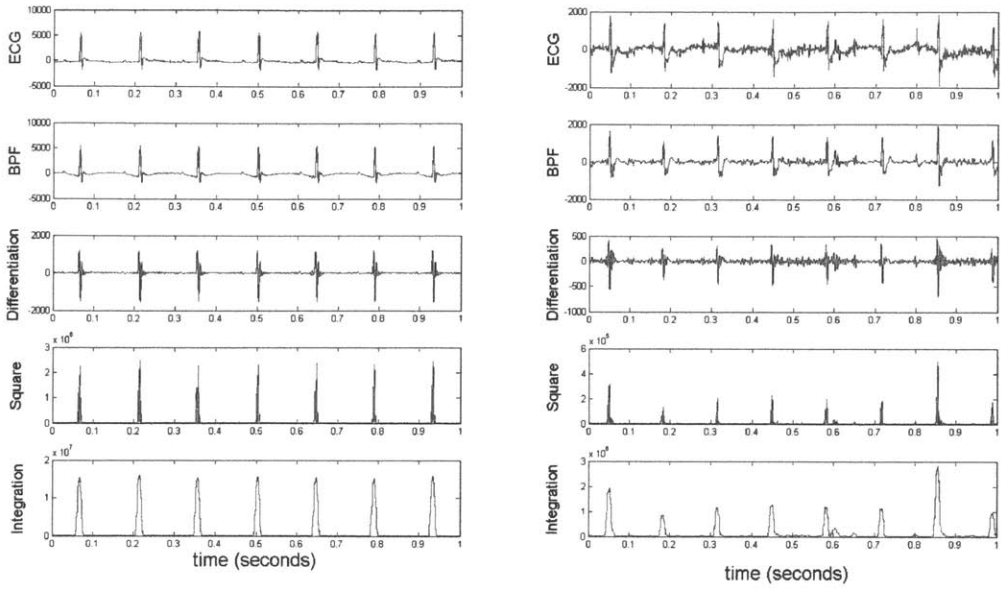

Figure 2-3: *Pan and Tompkins* algorithm pre-processing. Clean (left figure) and noisy ECG (right figure). From top to bottom on each figure: original mouse electrocardiogram (ECG), band-pass filtered ECG, differentiation, squaring and moving-window integration.

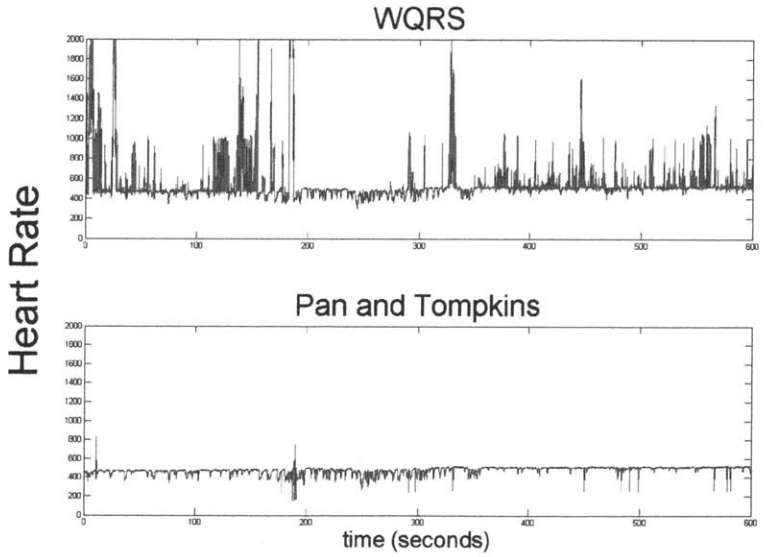

Figure 2-4: Beat-to-beat heart rate detected by *wqrs* (upper) and *Pan and Tompkins* (lower) algorithm on a noisy mouse ECG.

2.3.2 Ectopic Rejection

Since HRV analysis examines the beat-to-beat timing variations during normal sinus rhythm, ectopic beats can affect HRV by introducing artifacts into the computation of the time and frequency domain measures. In humans as well as mice, it is ideal that clinicians classify each beat. However, classifying each beat in long term ECG recording is very time consuming and impractical. Therefore, an ectopic or artifact rejection algorithm is needed to exclude these beats from the analysis.

One of the most common algorithms used in humans in identifying ectopic beats is adapted for the mouse. Beats assumed to be ectopic are determined by the fractional change of the $(n+i)^{th}$ RR interval (RR_{n+i}) from the most recent normal RR interval (RR_n). ΔRR_{n+i} is calculated as

$$\Delta RR_{n+i} = \frac{|RR_{n+i} - RR_n|}{RR_n}, \tag{2.1}$$

where n and i are integers.

If $\Delta RR_{n+i} > (i * 0.15)$, the $(n+i)^{th}$ beat is assumed ectopic resulting in the deletion of the $(n+i)^{th}$ and $(n+i+1)$ RR intervals. As an example, given that the n^{th} beat is normal, if ΔRR_{n+1} is greater than 0.15, RR_{n+1} and RR_{n+2} intervals are deleted. The next RR interval RR_{n+3} is then compared to RR_n. If ΔRR_{n+3} is greater than $3 * 0.15$, RR_{n+3} and RR_{n+4} intervals are deleted. The algorithm is assumed to remove some sinus beats as well as retain a few ectopic beats. The threshold of 0.15 is arbitrary and is similar to the threshold used in humans [25, 26]. Furthermore, 30 second segments with fewer than 50 beats after ectopic deletion are discarded from the analysis.

2.4 HRV Parameters

HRV is evaluated using time and frequency domain analysis. To perform the analysis, an RR tachogram is obtained using the output of the *Pan and Tompkins* algorithm discussed above. Additionally, since only normal-to-normal beats are considered for

the analysis, the RR tachogram is filtered by the ectopic beat detection algorithm. It should be noted that the RR tachogram is an unevenly sampled time series. Since mouse heart rate and respiratory rate is approximately 10 times faster than humans, some of the HRV metrics used in humans will be scaled by a factor of 10 to be applicable to mice [4].

2.4.1 Time Domain

In the time domain, standard HRV indices mean (RR_{mean}) and standard deviation ($SDNN$) of the RR intervals are computed. The time domain indices will be calculated as follows:

Given there are N RR intervals in a segment,

1. Mean

$$RR_{mean} = \frac{1}{N}\sum_{n=1}^{N} RR_n \tag{2.2}$$

2. Standard Deviation

$$SDNN = \sqrt{\frac{1}{N-1}\sum_{n=1}^{N}(RR_n - RR_{mean})^2} \tag{2.3}$$

2.4.2 Frequency Domain

Power spectral analysis is a widely used technique to assess activity of the autonomic nervous system [12]. As mentioned before, considering the differences in heart rate and respiratory rate between mice and humans, the frequency spectrum of the RR tachogram is split in three frequency bands:

- VLF - very low frequency — $<$ 0.4 Hz.
- LF - low frequency — 0.4 Hz - 1.5 Hz.
- HF - high frequency — 1.5 Hz - 5 Hz.

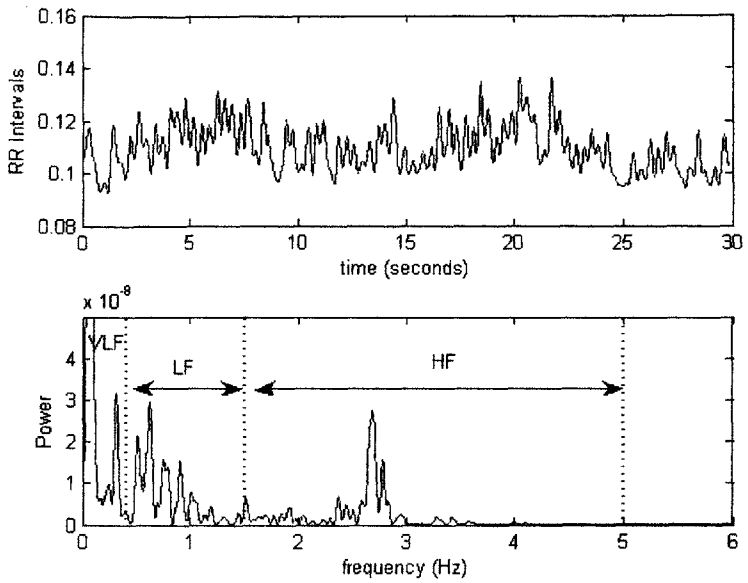

Figure 2-5: *Welch*'s averaged periodogram. A 30 second RR tachogram (upper) and the power spectrum (lower).

Normalized power within the low (LF) and high (HF) frequency bands as well as the $\frac{LF}{HF} ratio$ are computed. Normalization of these parameters is as follows:

$$LF_{norm} = \frac{LF}{LF + HF} \tag{2.4}$$

$$HF_{norm} = \frac{HF}{LF + HF} \tag{2.5}$$

Power spectrum is estimated using *Welch*'s average periodogram [27]. However, due to the uneven sampling nature of the RR tachogram, it needs to be interpolated and resampled. The RR intervals are interpolated using cubic spline interpolation and resampled at a sampling frequency of 30 Hz. Therefore, in a 30 second window, there are 900 sample points. These points are divided into 8 overlapping segments of 200 points each. Each segment will be zero padded to 256 points and eight periodograms are computed and averaged to estimate the power spectrum.

2.5 Activity Index

Physiological state is needed to compare HRV indices in different segments. In this thesis, an ECG derived activity index is used to estimate physiological state of the mouse. The components of the activity index involve heart rate, ECG noise and the cross-spectral density between the respiratory sinus arrythmia (RSA) and ECG derived respiration (EDR).

2.5.1 Noise Content in ECG

Increase in noise in the ECG signal is a strong indication of an increase in level of physical activity. ECG noise is estimated by power spectral analysis using the fast fourier transform (FFT). Specifically, *Welch's* averaged periodogram method is used . In particular, on a given discrete time ECG signal, the mean is removed and linearly detrended. The signal is then divided into eight sections with 50% overlap. Each section is windowed with a Hamming window, zero padded to the next power of two and eight periodograms are computed and averaged.

The energy in the clean mouse ECG signal is mostly contained between 1 Hz to 200 Hz (see Fig. 2-6). In Figure 2-6, it should be noted that the first peak in the power spectrum corresponds to the mouse heart rate. A noisy mouse ECG signal usually results in an increase in energy in the low (< 3 Hz) frequency range which corresponds to baseline wander of the ECG (see Fig. 2-7). Surprisingly, noise in the ECG signal, which includes movement and muscle artifacts, does not seem to manifest itself as a significant increase in energy above 200 Hz. For this reason and due to the fact that mouse (dKO) heart rate can drop below 120 (below 2 Hz), ECG noise will be measured primarily by baseline wander (energy below 1 Hz). Specifically, the ECG index is measured as

$$ECG_{index} = \frac{Power > 1\,Hz}{Total\ Power\ (0 - 250\,Hz)} \tag{2.6}$$

Therefore, equation 2.6 will have a value between 0 and 1, where a value of 1 indicates noise free (no baseline wander) ECG signal and a value closer to 0 for very

noisy ECG.

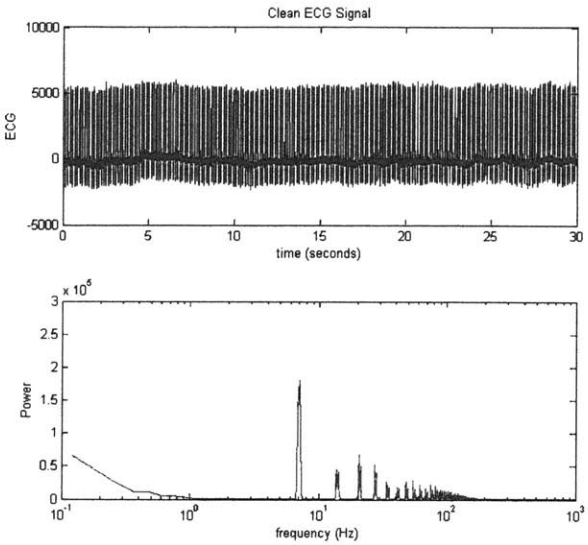

Figure 2-6: A 30 second segment of a clean mouse ECG (top). Power spectrum of the clean ECG signal (bottom). Note that peak in the power spectrum around 7 Hz corresponds to the mouse heart rate (420 bpm).

2.5.2 RSA and EDR

Heart rate increases with inspiration and decreases with expiration. This phenomenon is known as respiratory sinus arrhythmia (RSA). RSA is *partly* due to the expansion and contraction of the lungs and the cardiac filling volume from variations of intra-thoracic pressure [8]. During inspiration, the pressure within the thorax decreases and venous return increases which stretches the right atrium resulting to a reflex increase in heart rate. The opposite happens during expiration. This is called the *Bainbridge reflex* [8].

Respiratory rate may be derived from the body surface ECG (EDR) by measuring the fluctuation of the mean cardiac electrical axis [22] or peak QRS amplitudes which accompany respiration. This fluctuation is due to changes in thoracic impedance caused by the expansion and contraction of the chest during respiration. Figure 2-8

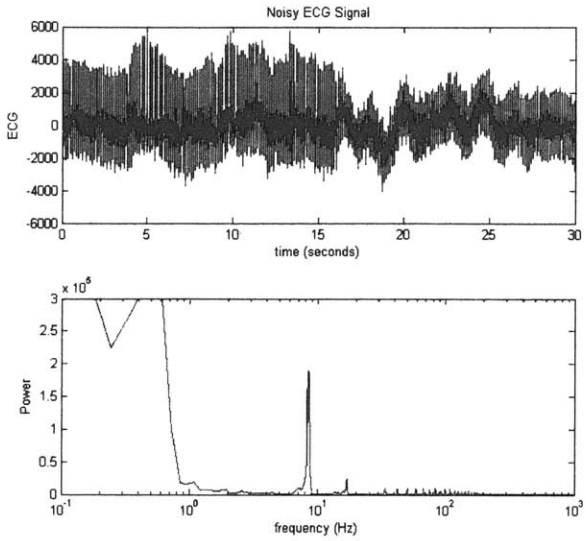

Figure 2-7: A 30 second segment of a noisy mouse ECG (top). Power spectrum of the noisy ECG signal (bottom). Note the increase in energy in the low frequencies.

shows RSA (RR interval oscillations) and EDR obtained from peak QRS amplitude in mice.

The frequency coupling of the two signals (RSA and EDR) is of great interest since it has been shown to be correlated to sleep stability in humans [23]. In this thesis, the frequency coupling of RSA and EDR is used as one of the major components in estimating mouse activity. Coupling between these two signals is more evident or easily obtainable when the mouse is at rest (or in deep sleep) where there are fewer factors that may significantly influence the heart rate or the ECG signal. Furthermore, the strongest coupling frequency will be directly correlated with respiration, which is a very good index of activity. Normal young adult mice have respiratory rate around 3 Hz.

Frequency coupling is measured using the cross-spectral density between RSA and EDR. Two slightly different measures of cross-spectral density are obtained: coupling frequency with respect to magnitude of the sinusoidal oscillations $A(f)$ and the consistency phase of the oscillations $\Theta(f)$ are separately calculated (details in appendix). Additionally, $A(f)$ and $\Theta(f)$ are normalized and multiplied together

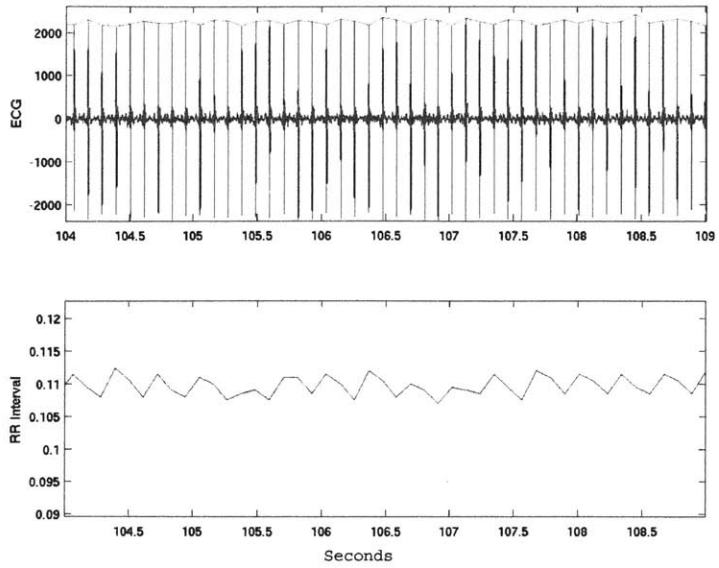

Figure 2-8: Respiratory Sinus Arrhythmia (RSA) and ECG derived respiration (EDR). EDR obtained from peak QRS amplitude (top) and RSA (bottom). Sinusoidal frequency of both plot are approximately 3 Hz.

to obtain *cardiorespiratory coupling* (CRC), a measure of RSA and EDR coupling. Mathematically,

$$CRC(f) = \frac{A(f)}{\max[A(f)]} * \frac{\Theta(f)}{\max[\Theta(f)]} = A_{norm}(f) * \Theta_{norm}(f) \tag{2.7}$$

CRC values range between 0 and 1, where the value closer to 1 means strong coupling of RSA and EDR at a given frequency. In Figure 2-9, CRC in a normal mouse, is plotted as a function of time. Notice that CRC sometimes peaks around the 3 Hz breathing frequency. Figure 2-10 shows the mean heart rate, ECG noise, maximum CRC in frequencies between 1.5 Hz to 5 Hz (CRC_{index}) greater than 0.4 and the corresponding frequencies. Observe that the regions where CRC_{index} is greater than 0.4 correlates with low mean heart rates and low ECG noise. Moreover, the corresponding frequencies are around 3 Hz, which is the normal breathing frequency. This observation indicates that CRC may be used as a good index of mouse activity.

It is important to note that frequency components of RSA and EDR signal can

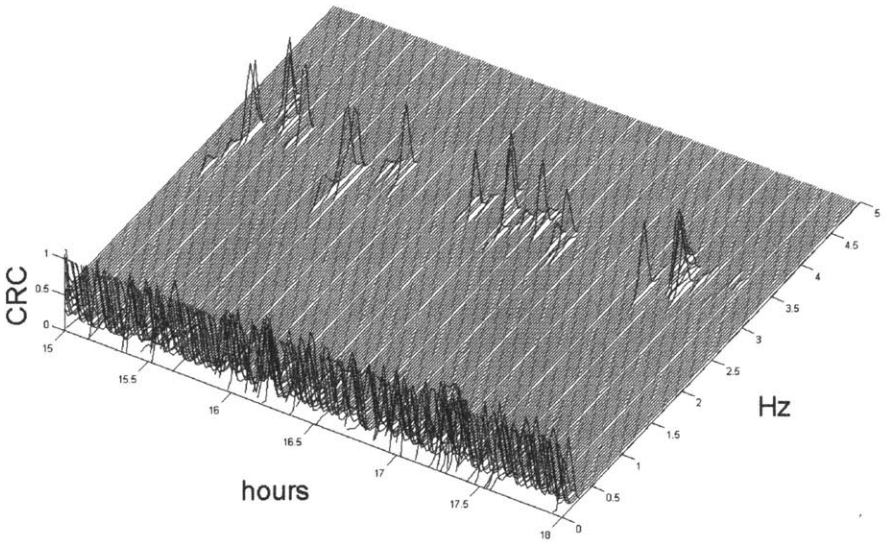

Figure 2-9: Cardiorespiratory Coupling (CRC). 3-D plot of CRC of a normal mouse. CRC is computed on a 30 second window and sliding the window by 45 seconds.

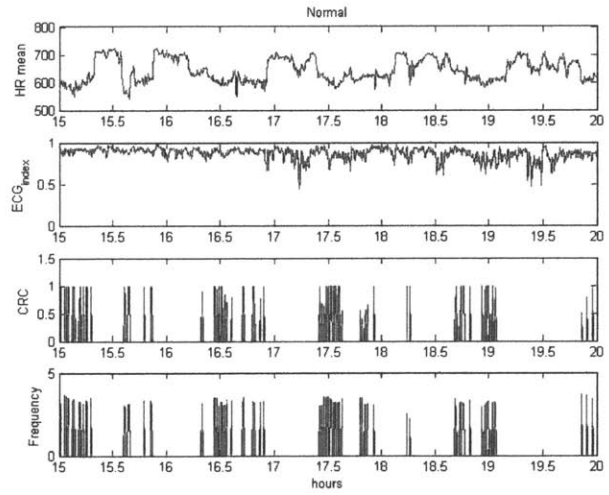

Figure 2-10: From top to bottom: mean heart rate HR_{mean} (bpm), ECG noise, CRC_{index} greater than 0.4 and frequency. Notice the correlation between high CRC_{index} with low heart rate and low ECG noise. CRC is computed on a 30 second window and sliding the window by 15 seconds.

only be obtained if heart rate is high enough (i.e. sampling effect of heart rate with respect to RSA and EDR). In the dKO mouse, extreme drop in heart rate can result in frequency aliasing. In figure 2-11, as HR_{mean} decreases the corresponding frequency of $CRC_{index} > 0.4$ also decreases until CRC_{index} eventually disappears (close to zero). It is unclear if the decrease in frequency is due to a decrease in heart rate (low sampling frequency) or the actual respiratory rate.

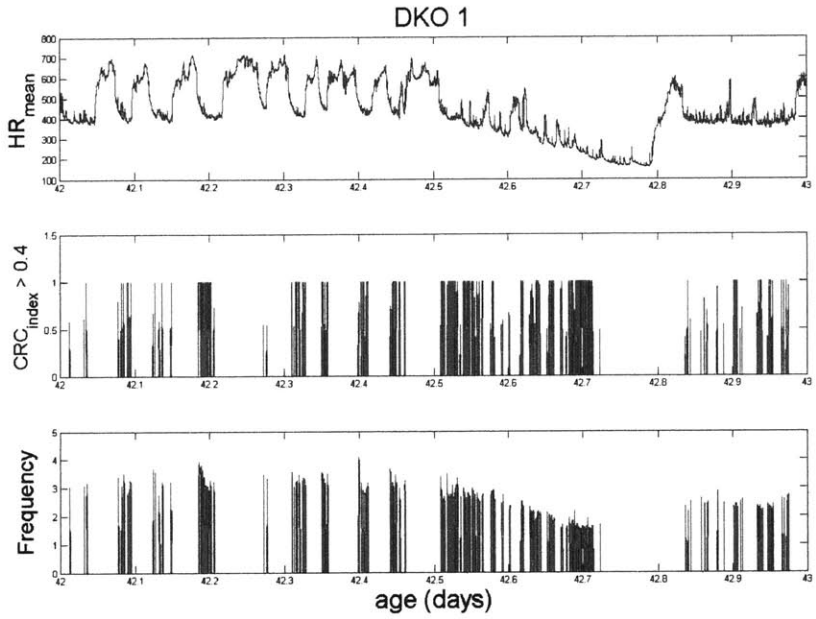

Figure 2-11: Mean heart rate HR_{mean} (bpm) (top), $CRC_{index} > 0.4$ (middle) and the corresponding frequency of the $CRC_{index} > 0.4$ of a dKO mouse.

2.5.3 Video Monitoring and Motion Detection

A video monitoring system with motion detection is necessary to track mouse activity and confirm the ECG derived activity index discussed in previous sections. Commercially available webcams, made by D-Link, are used for image acquisition. These webcams have a built in motion detector; however, the motion detection output cannot be easily extracted and correlated to the ECG signal. More importantly, the motion detection is set at a fixed sensitivity and outputs only binary decisions (i.e.

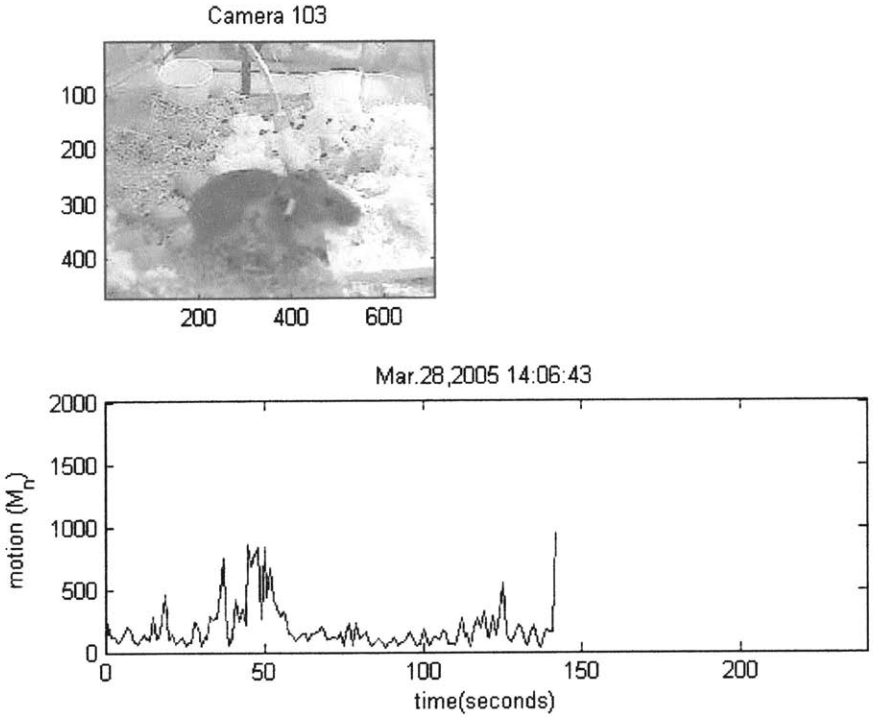

Figure 2-12: Real-time motion detection. Mouse image (upper) and motion M_n (lower) is plotted. High values of M_n indicate increased activity.

presence or absence of motion). These constraints are difficult to overcome especially for different image background, color and lighting.

In this thesis, a simple motion detection algorithm using mean squared difference between successive images is used. Specifically, given two N x M images X_{ij} and Y_{ij}, where i and j are coordinates for the ith and jth pixel respectively, motion M_n is calculated as

$$M_n = \frac{1}{NM} \sum_{i=1}^{N} \sum_{j=1}^{M} (Y_{ij} - X_{ij})^2 \tag{2.8}$$

Increased level of activity results in $M_n \gg 0$ while minimum activity decreases M_n towards 0 (see Fig. 2-12). Successive images are taken 1 second apart and M_n is calculated using Matlab (see Fig 2-12). Details of the algorithm implementation will be discussed in the appendix.

Chapter 3

Results

3.1 Overview

In this chapter, HRV variables in similar physiological states (activity index) are computed and possible trends are determined. Mouse HRV and physiological state are estimated for every 30 second epoch. The number of RR intervals in a 30 second time frame in mice corresponds to about a 5 minute time epoch in humans, which is the recommended length for short-term HRV analysis [1].

Daily (7am-7am) averages of the HRV indices including lights on (7am-7pm) and lights off (7pm-7am) are presented. The length of the data obtained ranges from five to nineteen days. The focus of this thesis is to determine if HRV has prognostic value in mice with CHD (dKO mice). Normal mice (wild type) are also used to look at similarities and differences in HRV. For normal mice, ECG recordings are terminated after ten days. However, in the dKO mice, recordings are discontinued immediately after they expire. Because of the possible effects of pain and anesthesia after surgical implantation of ECG electrodes, dKO mice that die less than 4 days after surgery are excluded. The Hermes identification numbers of all the mice used are located in the appendix.

3.2 HR_{mean} and $SDNN$

In figure 3-1, HR_{mean} ($\frac{60}{RR_{mean}}$) and $SDNN$ are plotted as a function of age in days. Mouse heart rate typically oscillates within a range of values on a given day (see Fig. 3-2). In the dKO mouse, HR_{mean} is statistically ($p < 0.01$, Student's T test) lower than the normal mouse (see Fig. 3-1, 3-2 and 3-3). In fact, HR_{mean} in normal mice is always greater than 400 bpm. In contrast, in the dKO group, HR_{mean} periodically drops below 400 bpm (see Fig. 3-1). Figure 3-4 shows the daily percentage of $HR_{mean} < 400$ bpm in dKO mice.

$SDNN$ in the dKO mouse is slightly higher than the normal mouse but not statistically significant (see Fig. 3-7). In figure 3-2, a close up view of HR_{mean} and $SDNN$ is shown. Observe that as HR_{mean} decreases $SDNN$ increases. Decreasing heart rate is a result of a shift in sympathovagal balance towards the parasympathetic component of the autonomic nervous system. This observation is consistent with the study done by Gehrmann *et. al.* [4]. As seen in figure 1-13, after sympathetic blockade, this results in a decrease in heart rate and an increase in $SDNN$.

In most dKO mice (4 out of 6), daily averages of HR_{mean} (figure 3-3) continue to decrease as the heart disease progresses and reaches minimum around the day they expire. Others die of sudden death possibly due to a massive MI. This event is captured in one of the dKO mice. In figure 3-5, notice that this mouse had a sudden drop in heart rate around the 34^{th} day of life and expired. The ECG shows heart block followed by ST segment elevation (see Fig. 3-6).

Daily average of $SDNN$ seems to increase in 3 dKO mice (see Fig. 3-7). This observation is not consistent with a study done in humans who survived an acute myocardial infarction (AMI) [2]. In the human study, patients with higher $SDNN$ after an AMI are more likely to survive. However, humans with poor prognosis usually develop congestive heart failure (CHF). It has not been documented that the dKO mice also develop CHF.

In the following sections, HRV metrics are measured in similar physiological states using ECG derived activity index discussed in the previous chapter. Boundaries

for the components of the activity index are determined and examples as well as illustrations are presented.

3.3 Activity Index and Motion Detection

In order to determine the boundaries or thresholds for the components of ECG derived activity index, simultaneous ECG and image recordings are done in a normal (wild type) and dKO mouse. Mean heart rate (HR_{mean}), ECG_{index}, motion index M_n and CRC_{index} are calculated and plotted in figure 3-8. Notice that increasing values of M_n are consistent with higher HR_{mean} and low values of ECG_{index} as well as CRC_{index}. Similarly, the opposite is true for decreasing values of M_n. It is important to point out that absence of ECG noise (ECG_{index} close to 1) does not always translate to decreasing activity (see lower plot in figure 3-8). Motion and movement artifacts are sometimes not seen on the ECG due to good electrode placement.

As mentioned in the previous chapter, the components for activity index involve heart rate, ECG_{index} and CRC_{index}. However, since the range of HR_{mean} is different for each mouse especially for dKO's, using a threshold for the HR_{mean} is not a reliable determinant for activity. For this reason, HR_{mean} is excluded as one of the components of activity index. Fortunately, HR_{mean} is not a big factor since high CRC_{index} and ECG_{index} usually correspond to low HR_{mean} in both normal and dKO mice (see Fig. 3-8).

In figure 3-9, scatter plots of ECG_{index}, CRC_{index} and 30 second average of motion M_n are shown. The average M_n is used because ECG_{index} and CRC_{index} are computed in 30 second segments while M_n is calculated every second. Reasonable thresholds for ECG_{index} and CRC_{index} are $\mathbf{ECG_{index} > 0.7\ AND\ CRC_{index} > 0.4}$. The physiological state of the mouse is assumed to be **sleep** during the 30 second segment that satisfies both conditions (see Fig. 3-9) [23]. The number of sleep segments detected in each group are plotted in figure 3-10 and 3-11. Notice that some dKO mice have less periods of sleep than the normal group. In addition, the number of sleep segments in normal mice are relatively stable across all days compared to the

dKO group. Moreover, since mice are nocturnal animals, there are less sleep segments detected at night in normal mice. However, the dKO mice seem to have more sleep segments during dark periods.

3.4 Heart Rate Variability in Sleep

In this section, HRV variables are calculated in physiological states assumed to be sleep. Sleep states of the mouse are estimated by the ECG_{index} and CRC_{index} using the conditions stated above. Daily, lights on, and lights off averages of HRV metrics during sleep are plotted in bar graphs and shown in this section on both normal and dKO mice.

3.4.1 Time Domain

Figure 3-12 and 3-13 shows average HR_{mean} and $SDNN$ bar graphs. Increasing $SDNN$ in 3 dKO mice (DKO 1, 2 and 3) and 2 normal (Normal 3 and 4) mice are visible in figure 3-13. There are no significant differences in average $SDNN$ in both groups.

Average HR_{mean} in the dKO mice is significantly lower than the normal group. In addition, some dKO mice have a decreasing trend in average HR_{mean} towards the end of life (DKO 3, 4, 5 and 6). Furthermore, during the final days before these mice expire, lights out averages are mostly lower than lights on averages. This indicates that bradycardic events in dKO mice occurs during dark periods. Bradycardic episodes are sometimes caused by a 2 to 1 heart block. The reason as to why these episodes often occur at night is unclear.

3.4.2 Frequency Domain

In the frequency domain, there are no identifiable trends in low frequency (LF_{norm}, Fig. 3-14) or high frequency (HF_{norm}, Fig. 3-15) power including the $\frac{LF}{HF}$ (Fig. 3-16) ratio in all dKO mice. There are also no significant differences in frequency

domain variables between dKO and normal mice. However, the $\frac{LF}{HF}$ ratio during lights on is higher than lights off in normal mice. This indicates a stronger sympathetic dominance during the lights on period in the normal group. This suggests that even though mice sleep more during daytime, they might spend less time in deep sleep compared to nights. The $\frac{LF}{HF}$ ratio in dKO mice seems opposite to that of the normal mice (i.e. $\frac{LF}{HF}$ ratio higher in dark period).

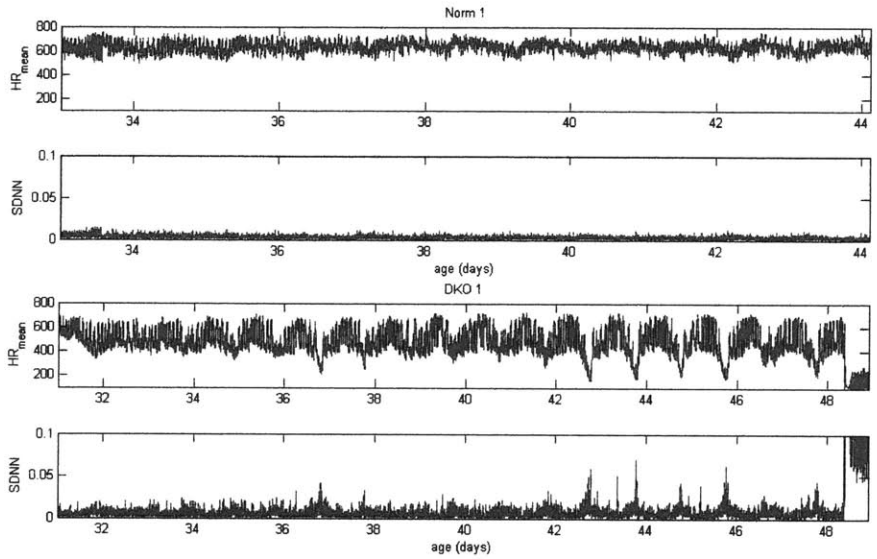

Figure 3-1: Mean heart rate HR_{mean} (bpm) (top) and standard deviation of RR intervals $SDNN$ (seconds)(lower) every 30 seconds in normal and dKO mouse.

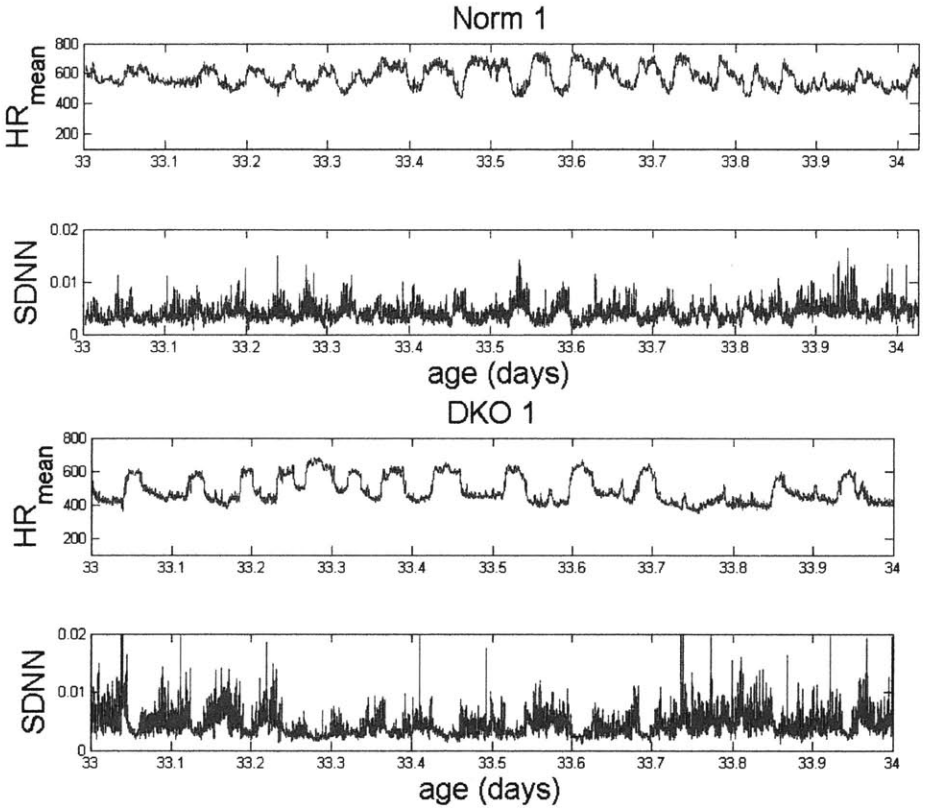

Figure 3-2: A closer view of mean heart rate HR_{mean} (bpm) (top) and standard deviation of RR intervals $SDNN$ (seconds) (lower) in normal and dKO mouse.

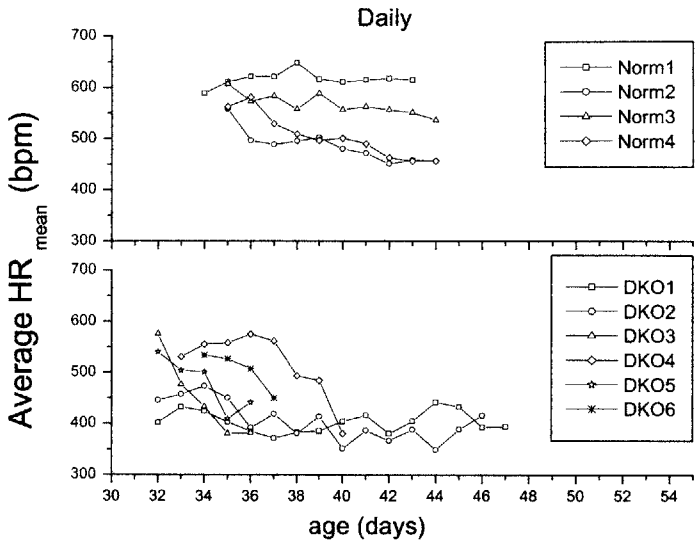

Figure 3-3: Daily (7am-7am) average HR_{mean}. Normal (upper) and dKO (lower) mice.

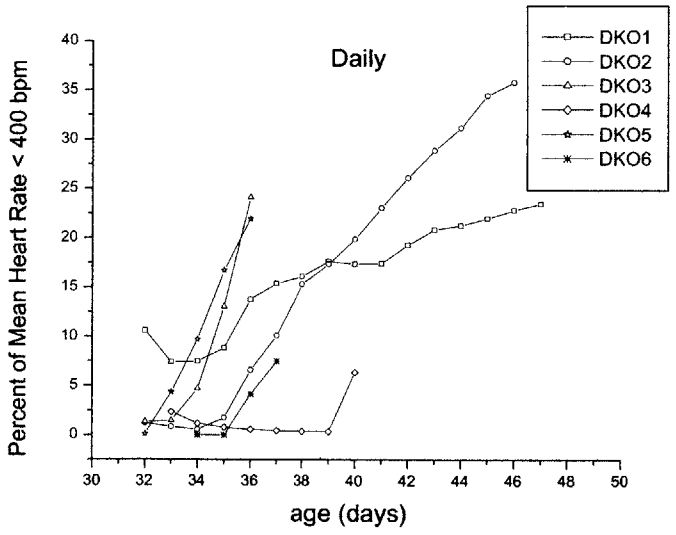

Figure 3-4: Daily (7am-7am) percentage of $HR_{mean} < 400$ bpm. HR_{mean} computes every 30 seconds.

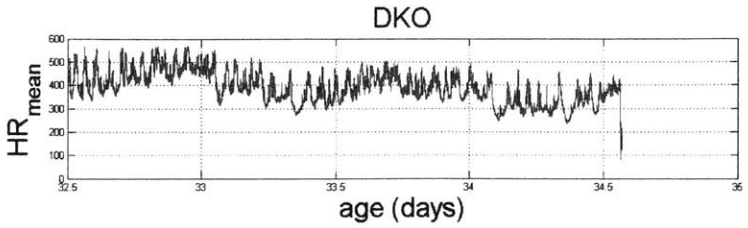

Figure 3-5: HR_{mean} of a dKO mouse. Notice the sudden drop in heart rate on the 34^{th} day of life.

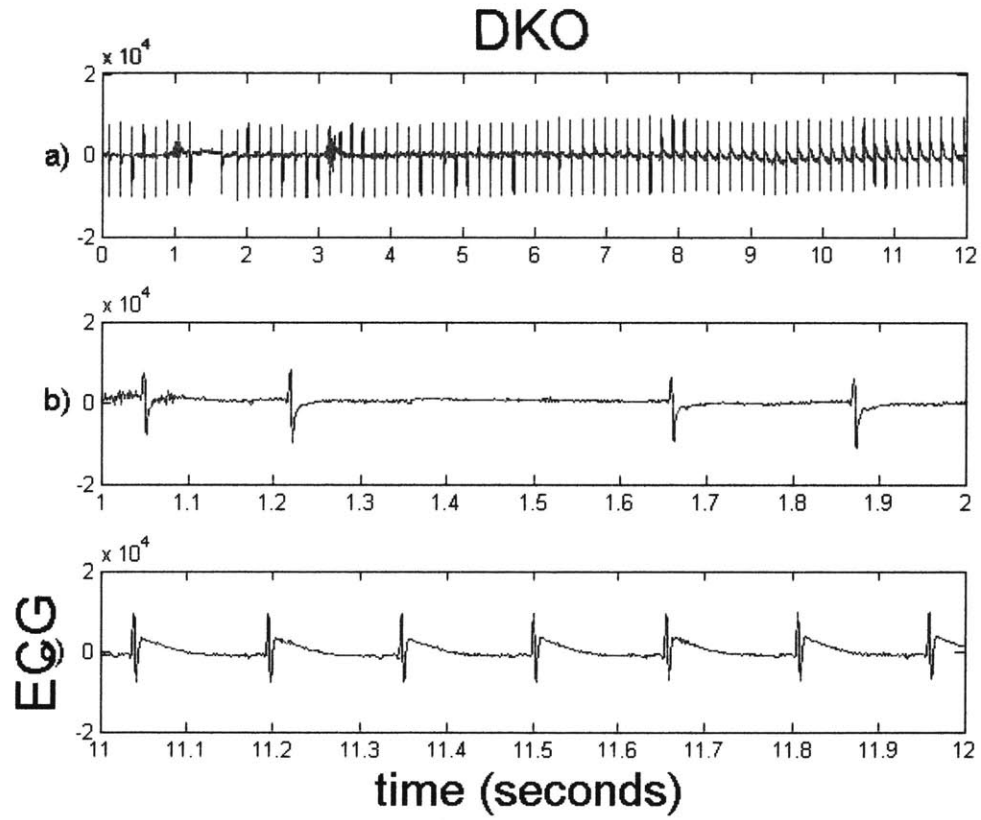

Figure 3-6: ECG of a dKO mouse. Heart block followed by an increase in ST segment shift. a) 12-second rhythm strip. b) Expanded view of seconds 1-2. Sinus pause followed by junctional escape beat. c) Expanded view of seconds 11-12. Sinus rhythm with ST segment elevation.

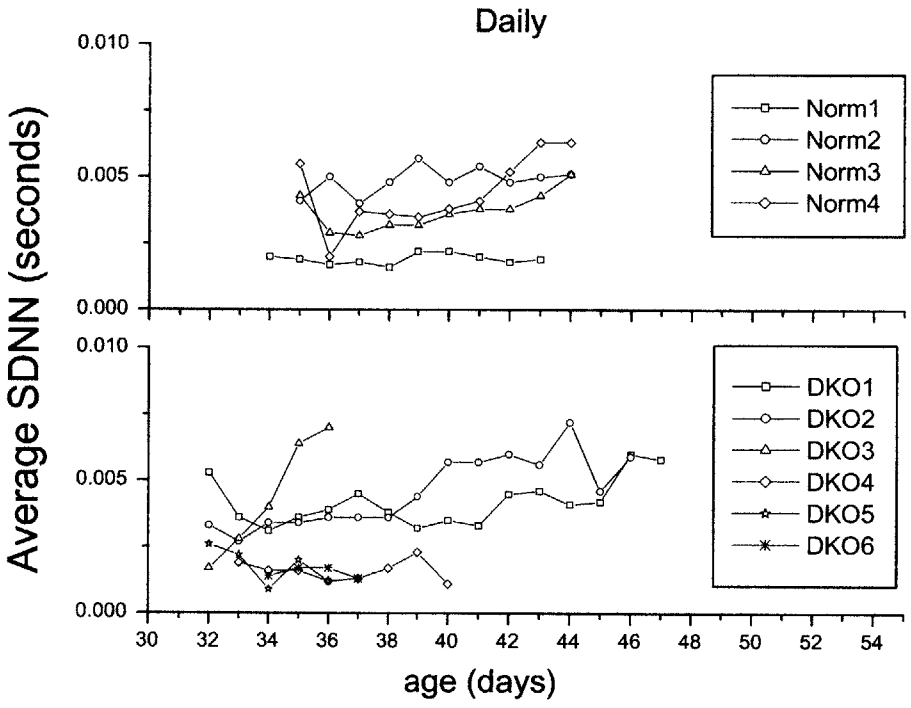

Figure 3-7: Daily (7am-7am) average $SDNN$. Normal (upper) and dKO (lower) mice.

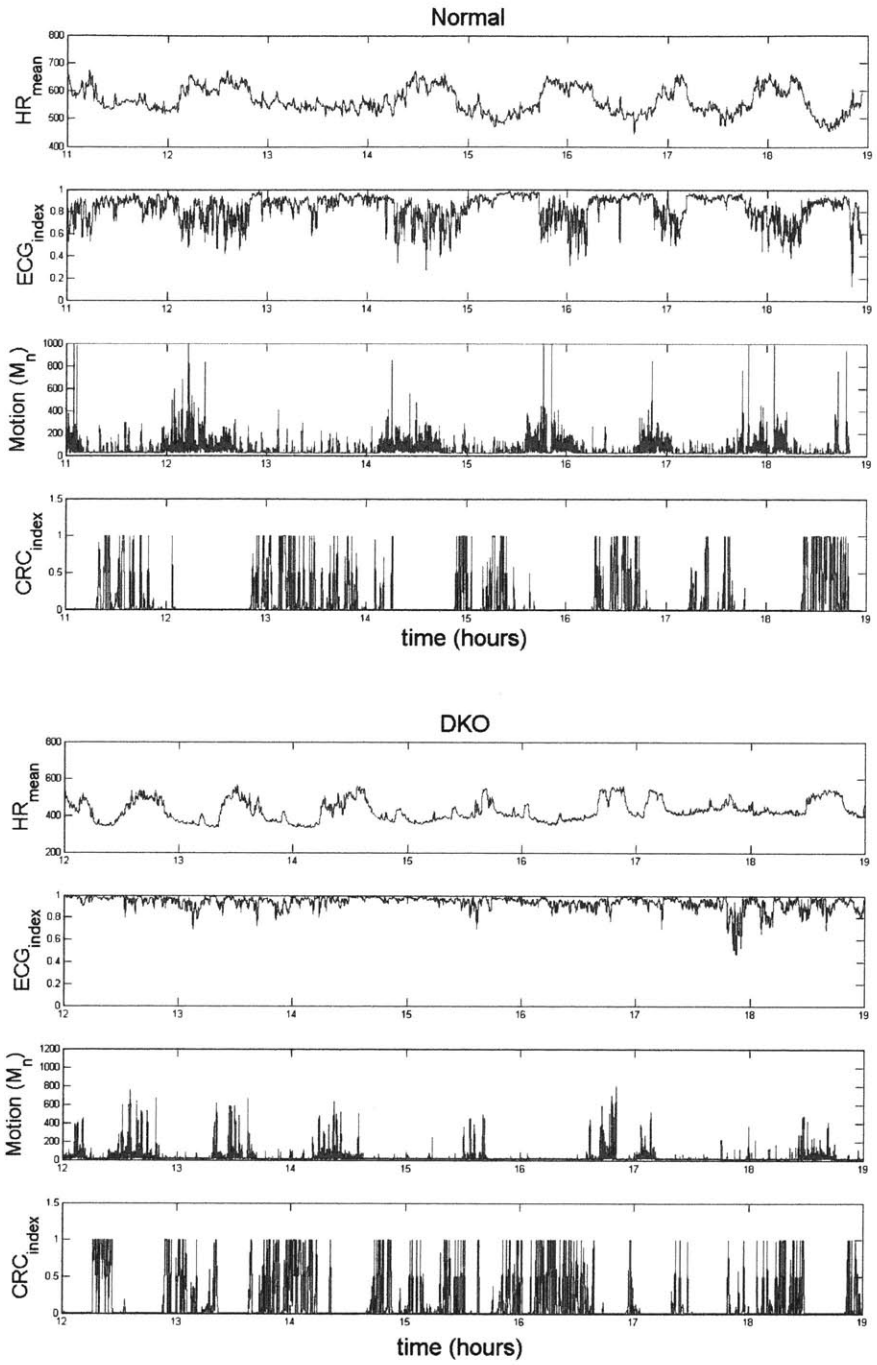

Figure 3-8: Normal mouse (upper figure) and dKO mouse (lower figure). From top to bottom: Mean heart rate HR_{mean} (bpm), ECG_{index}, motion M_n and CRC_{index}.

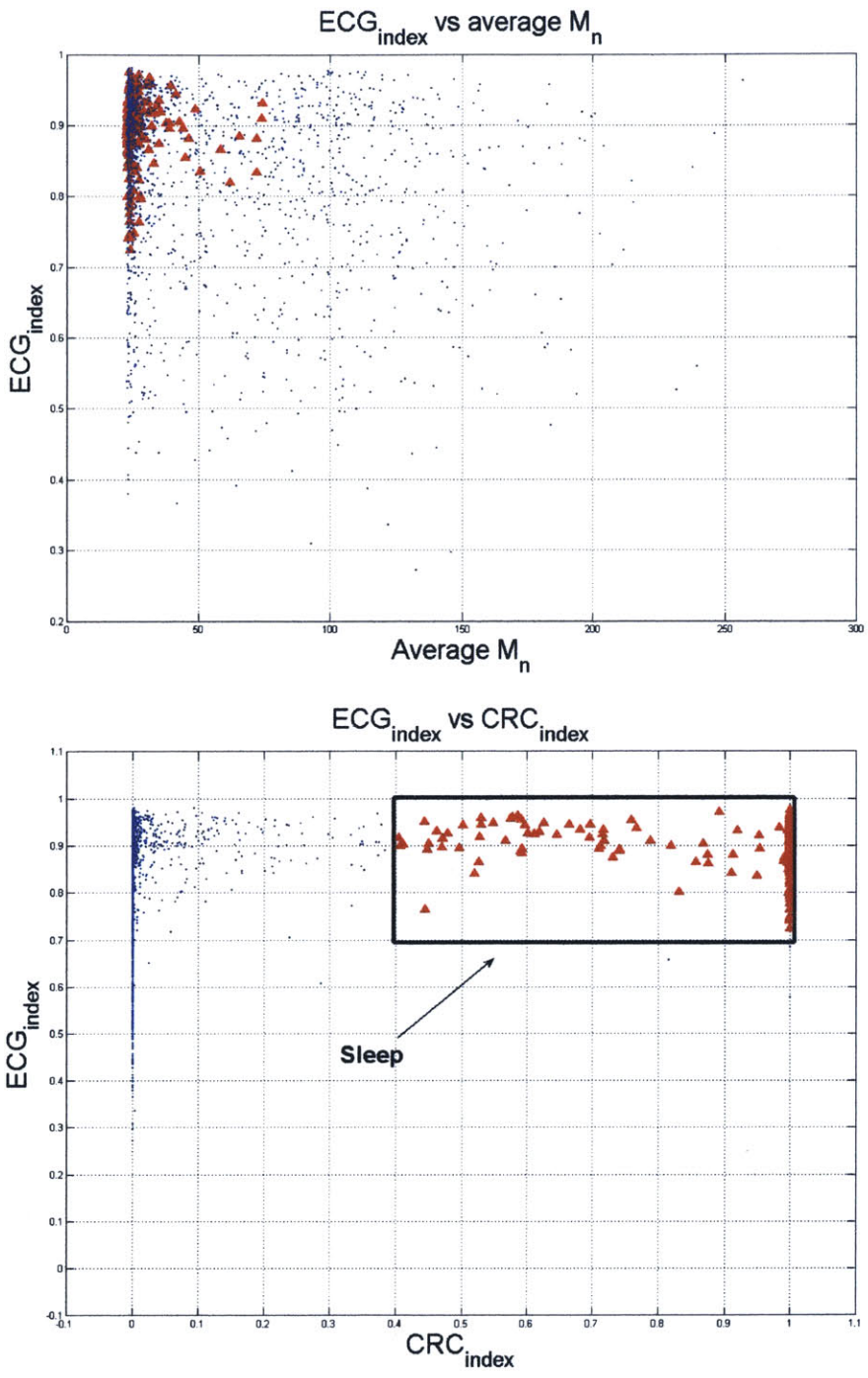

Figure 3-9: Scatter plot. ECG_{index} vs. average M_n (upper). Triangles represent data points that also have $CRC_{index} > 0.4$. CRC_{index} vs. ECG_{index} (lower). Points inside the rectangle in the bottom figure assumes the mouse is sleeping ($ECG_{index} > 0.7$ AND $CRC_{index} > 0.4$).

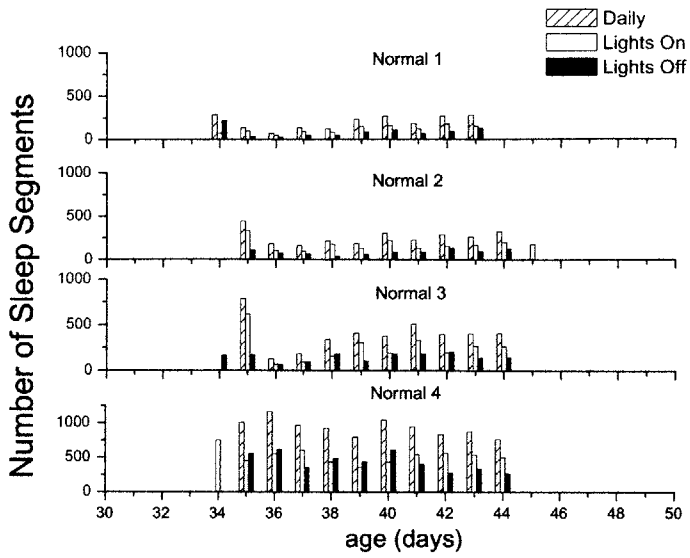

Figure 3-10: . Number of 30 second sleep segments detected in normal mice.

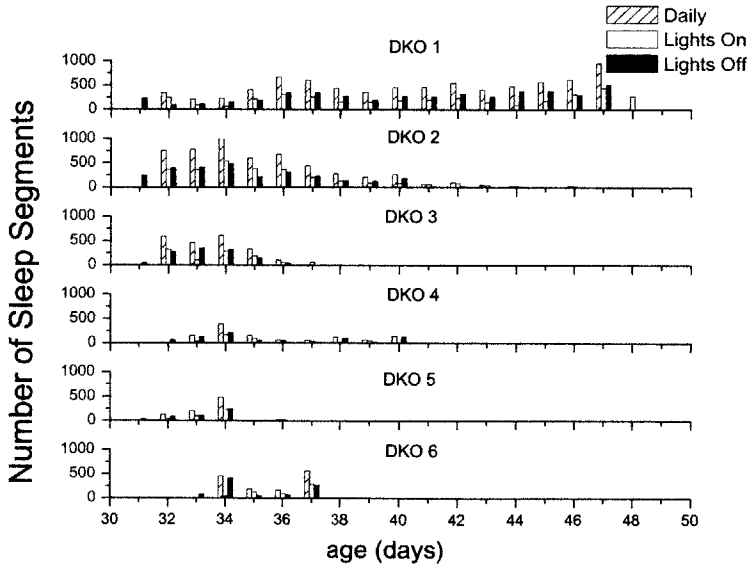

Figure 3-11: . Number of 30 second sleep segments detected in dKO mice.

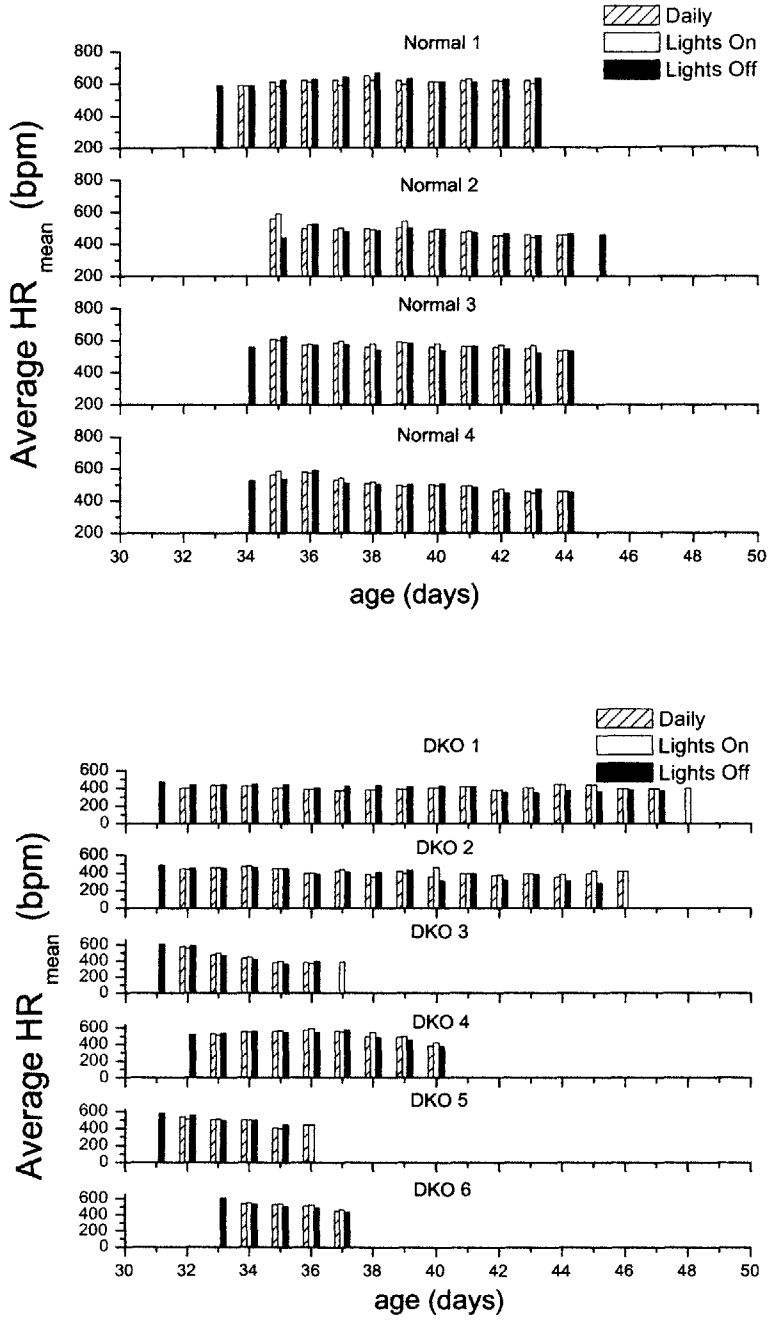

Figure 3-12: Daily (7am-7am), lights on (7am-7pm) and lights off (7pm-7am) HR_{mean} averages in normal (upper) and dKO (lower) mice during sleep.

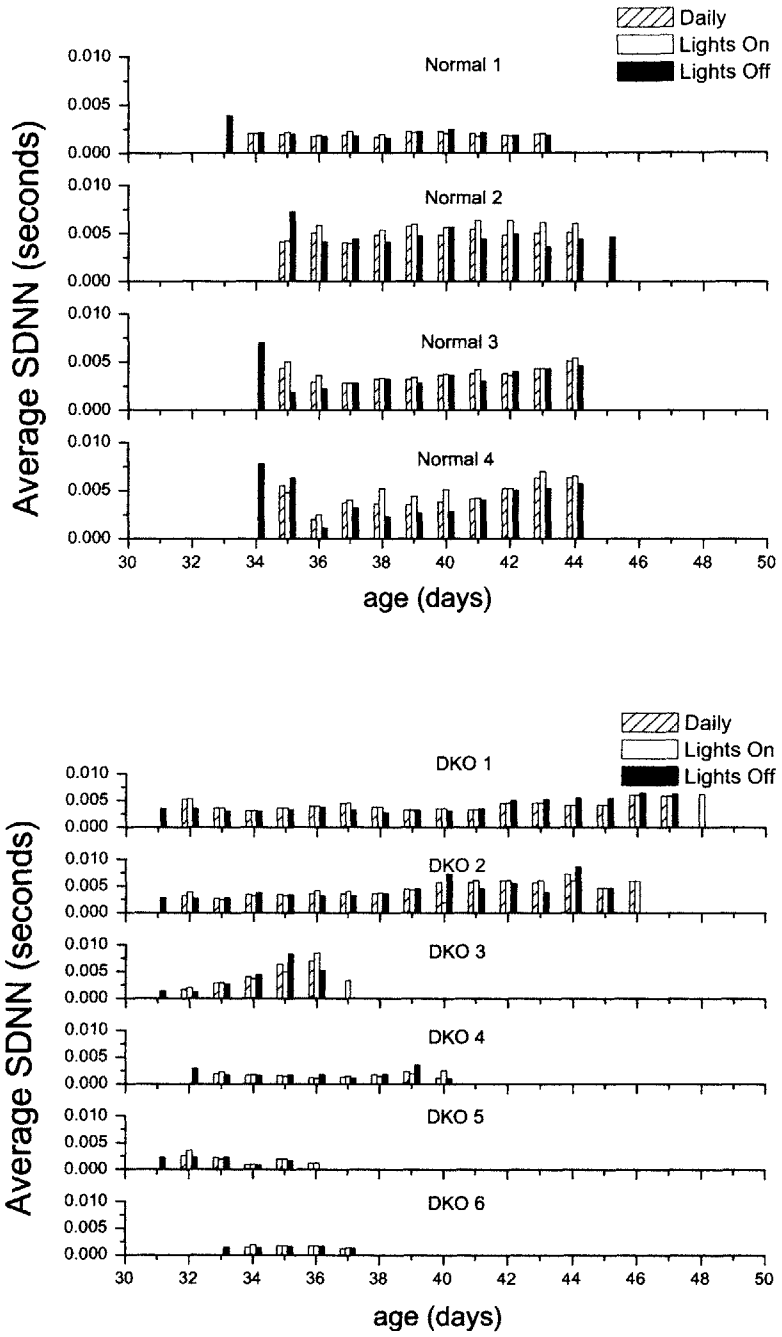

Figure 3-13: Daily (7am-7am), lights on (7am-7pm) and lights off (7pm-7am) $SDNN$ averages in normal (upper) and dKO (lower) mice during sleep.

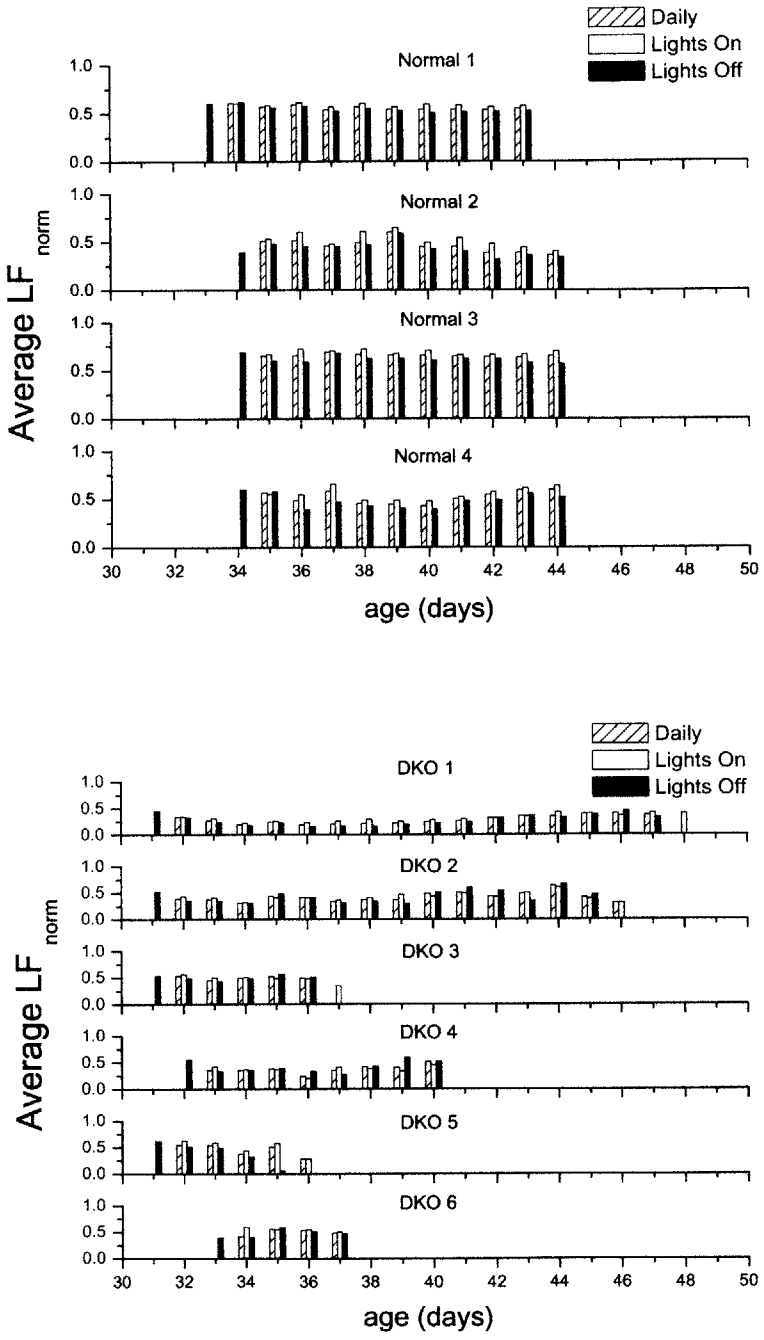

Figure 3-14: Low frequency (LF) power. Daily (7am-7am), lights on (7am-7pm) and lights off (7pm-7am) averages in normal and dKO mice during sleep.

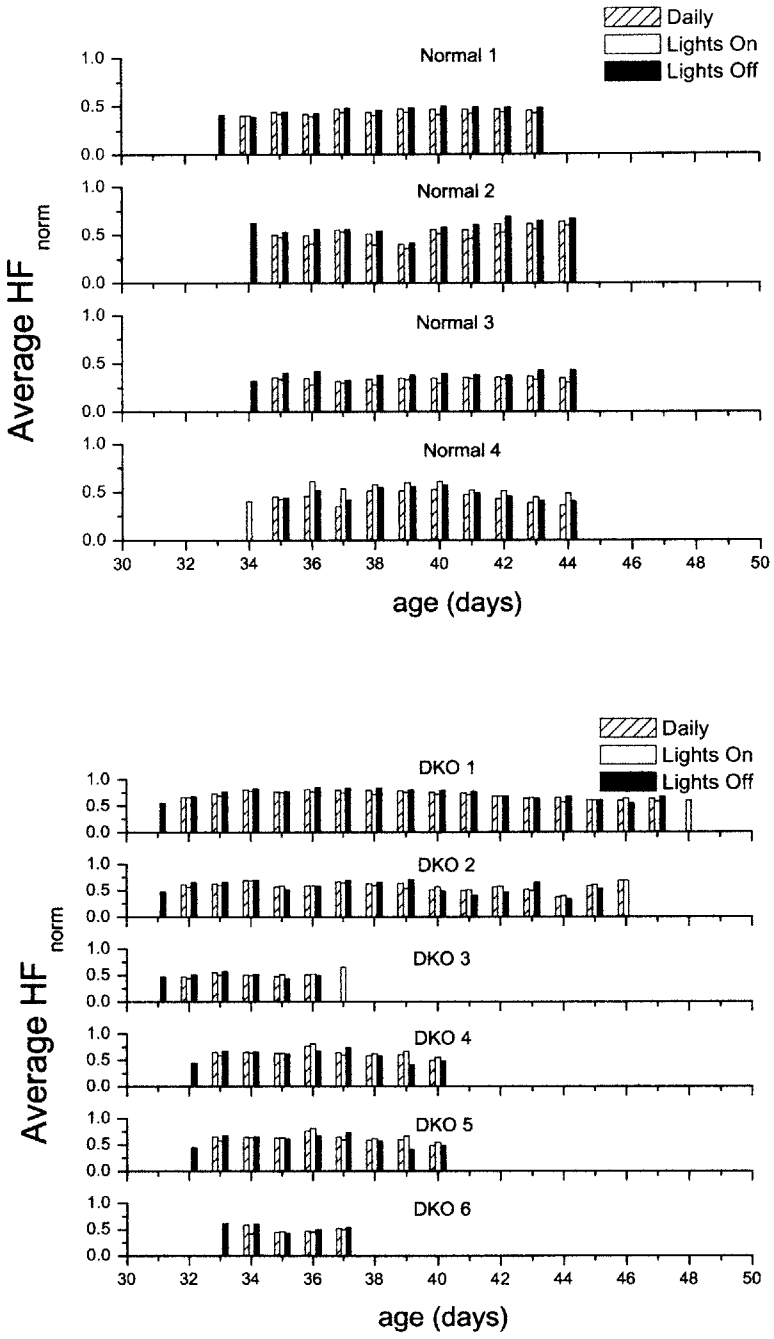

Figure 3-15: High frequency (HF) power. Daily (7am-7am), lights on (7am-7pm) and lights off (7pm-7am) averages in normal and dKO mice during sleep.

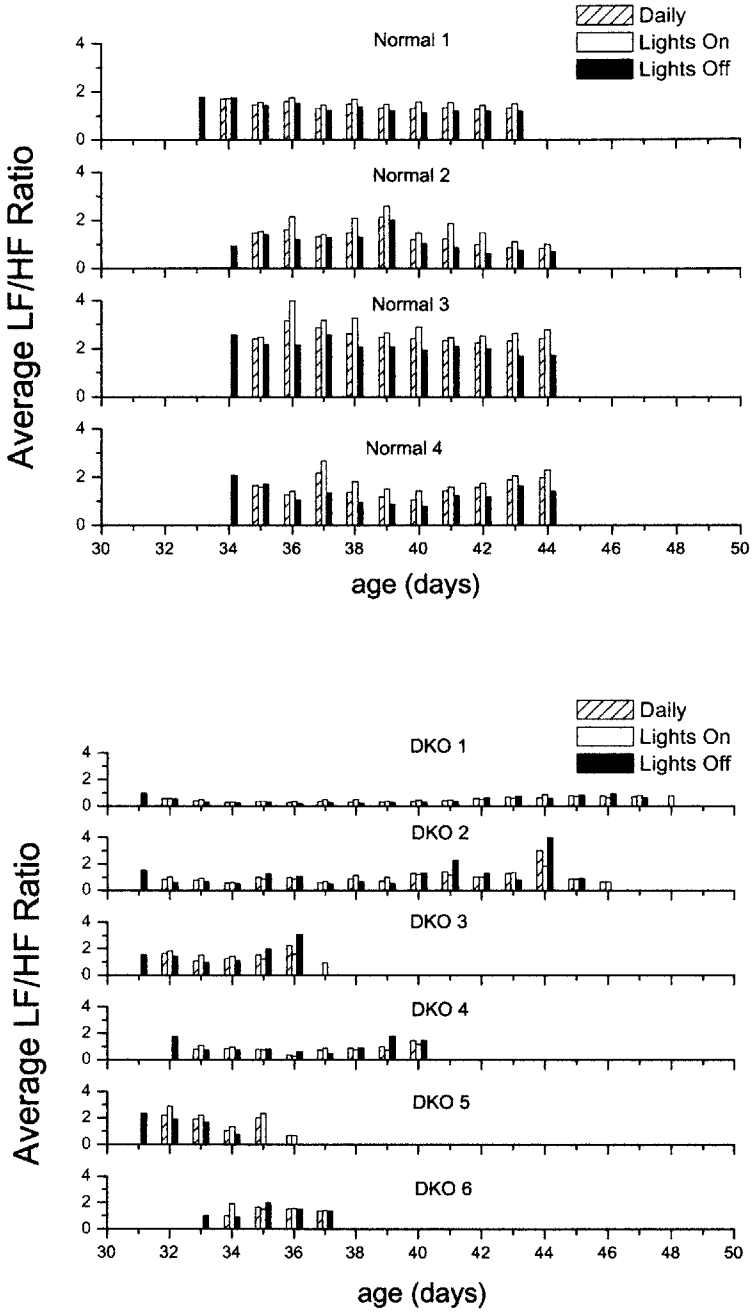

Figure 3-16: Low/high frequency ratio ($\frac{LF}{HF}$). Daily (7am-7am), lights on (7am-7pm) and lights off (7pm-7am) averages in normal and dKO mice during sleep.

Chapter 4

Discussion and Conclusion

Advances in genetic engineering have made the mouse the animal of choice to model human CHD. Genetically engineered dKO mice that exhibit similar symptoms as human CHD have been developed in the Kreiger lab at MIT [3]. In humans, the influence of myocardial ischemia and infarction on the autonomic control of the heart has been well investigated [2, 7, 14, 16, 18]. For decades, HRV has been used as a tool to assess activity of the autonomic nervous system. It has been found that depressed HRV is a powerful predictor of mortality in patients after an acute MI [2]. The physiological mechanism of decreased HRV is thought to reflect a shift in sympathovagal balance characterized by a relative sympathetic dominance and/or a reduced parasympathetic activity. Due to the prognostic value of HRV in humans, this thesis has studied the impact of CHD on the role of the autonomic nervous system on heart rate dynamics in the mouse model using HRV analysis.

Although there are accepted standards for measuring HRV metrics in humans, there are no such standards in mice. The calculation of HRV metrics in mice used in this thesis is based on human standards appropriately scaled by a factor of 10 due to heart and respiratory rate differences between the two species [4].

In chapter 2, the details of calculating traditional HRV variables were discussed including signal processing techniques to extract the RR interval time series and a method to estimate physiological state from the ECG. RR intervals were obtained using a mouse adapted version of *Pan and Tompkins* QRS detector. The *Pan and*

Tompkins QRS detector was shown to perform very well on mouse ECG and even better than the *wqrs* detector, especially for noisy segments.

In order to compare physiological measurements (HRV) at different times, it is always important to know the physiological state of the mouse. Chapter 2 described a novel method to estimate physiological state using ECG noise (ECG_{index}) and the coupling of the EDR and RSA signal (CRC_{index}). An activity index was developed by applying thresholds on both ECG_{index} and CRC_{index} which classified sleep and non-sleep states in the mouse. A motion detector using a commercially available camera was built to validate the ECG derived activity metric. It was found that this metric provided a reliable activity index.

In chapter 3, results of the HRV measurements were presented. As CHD progressed, there was no evidence of any identifiable trend in HRV metrics in the dKO mice. Time and frequency domain variables did not show any prognostic value. Mean heart rate (HR_{mean}) has shown some predictive power of mortality, but it was not consistent in all the dKO mice. However, HR_{mean} was the only metric that could separate dKO and normal mice. Normal mice had HR_{mean} that was always greater than 400 bpm while HR_{mean} in the dKO mice periodically dropped below this threshold (Fig. 3-4). Although some dKO mice die of sudden cardiac death, a few of them have a unique behavior characterized by about a 50% drop in heart rate that can last for a few hours followed by a recovery period that resets the heart to its normal rate (Fig. 3-1). Additionally, the bradycardic episodes usually occurred in dark periods. The mechanism behind this phenomenon is still a mystery.

In regards to the activity index to detect sleep, the number of sleep segments during the day were higher compared to night in normal mice. This observation was consistent since mice are known to be more active at night. However, this observation seems opposite in the dKO mice. The reason for this cannot be explained.

In the frequency domain, the $\frac{LF}{HF}$ ratio during the day was higher than at night in control mice. This could indicate that normal mice spent more time in deep sleep at night compared to daytime when they are less active. However, this ratio seemed to be reversed in the dKO mice. A possible explanation for this is that myocardial

ischemia and infarctions might have occurred more frequently at night which could be accompanied by an increase in sympathetic activity.

Finally, although it was found that HRV was not helpful in predicting mortality in dKO mice, future research might focus on using the activity index developed in this thesis in conjunction with other possible prognostic measure such as ST segment analysis. Also, the camera used in this thesis will be adapted to the Hermes Server to simultaneously monitor mouse activity and ECG. This will be very useful tool in future research on the dKO mouse.

Appendix A

Power and Cross-Spectral Density

The *Einstein-Wiener-Khinchin* theorem states that the power spectral density $S_{xx}(f)$ of a wide-sense stationary random process $X(t)$ is given by the Fourier transform of the its autocorrelation function $R_{xx}(\tau)$ [28]:

$$S_{xx}(f) = \mathcal{F}[R_{xx}(\tau)], \tag{A.1}$$

where $\mathcal{F}[.]$ indicates taking the Fourier transform.

In real applications, signals usually have one realization. Since power spectral density is a statistical measure, $S_{xx}(f)$ is commonly estimated using *Welch*'s method. This method is carried out by dividing the time signal into successive (sometimes overlapping) blocks and averaging the periodogram of the signal blocks. Let $P_{xx}^{i}(f)$ be the periodogram of the i^{th} block. Then the power spectral density can be estimated by

$$S_{xx}(f) = \mathcal{E}[|P_{xx}^{i}(f)|^2], \tag{A.2}$$

where $\mathcal{E}[.]$ denotes averaging across all blocks indexed by i. In general, $P_{xx}^{i}(f)$ is always real for all i's.

The notion of power spectral density can also be generalized to two jointly wide-sense stationary process $X(t)$ and $Y(t)$ [28]. The cross-spectral density $S_{xy}(f)$ is defined by

$$S_{xy}(f) = \mathcal{F}[R_{xy}(\tau)], \tag{A.3}$$

where $R_{xy}(\tau)$ is the cross-correlation between $X(t)$ and $Y(t)$.

The *Welch*'s method in equation A.2 can also be applied to estimate the cross-spectral density. However, the order in which to take the squaring and averaging have a significant impact on the results. The cross-spectral density can be calculated in two ways:

$$A(f) = \mathcal{E}[|P^i_{xy}(f)|^2] \tag{A.4}$$

and

$$\Theta(f) = |\mathcal{E}[P^i_{xy}(f)]|^2, \tag{A.5}$$

where $P^i_{xy}(f)$ is the cross-periodogram of the i^{th} block. In general, $P_{xy}(f)$ is complex even if $X(t)$ and $Y(t)$ are real. Since $A(f)$ is calculated by taking the magnitude squared of $P_{xy}(f)$ in each block followed by averaging, it corresponds to the frequency coupling of the two signals due to the oscillation amplitudes only. Similarly, since $\Theta(f)$ is computed by first averaging the real and imaginary parts of $P_{xy}(f)$ across all blocks followed by magnitude squaring, it measures the consistency in phase of the oscillations across all blocks. $A(f)$ and $\Theta(f)$ is used as a measure for *cardiorespiratory coupling* (CRC) in equation 2.7. The calculation of CRC is slightly different than the *cardiopulmonary coupling* (CPC) in [23].

A.1 A Simple Example

$x_1(t)$ and $y(t)$ are sinusoidal signals with a frequency of 1 Hz and 3 Hz respectively. Also, $x_2(t)$ is a sinusoidal signal with the same frequency as $x_1(t)$ with an offset at 10 and 20 seconds (see Figure A-1).

Let,

$z_1(t) = x_1(t) + y(t)$ and

$z_2(t) = x_2(t) + y(t)$.

The two signals, $z_1(t)$ and $z_2(t)$, are then divided into 3 sections (0-10, 10-20 and 20-30 seconds). $A(f)$ and $\Theta(f)$ between $z_1(t)$ and $z_2(t)$ are computed and plotted in figure A-2. Observe that $\Theta(f)$ at 1 Hz is lower due to the phase inconsistency of $x_2(t)$. Note that $A(f)$ will be equal to the power spectral density of the signal $z_1(t)$.

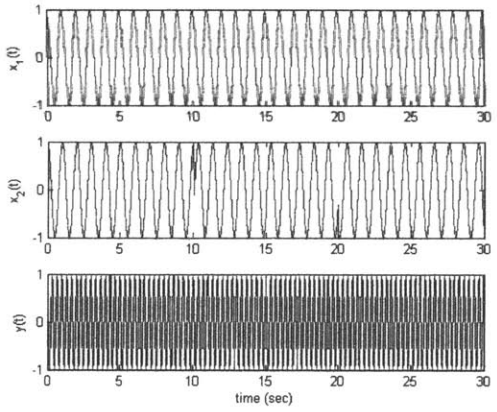

Figure A-1: $x_1(t)$ (top), $x_2(t)$ (middle) and $y(t)$ (bottom). Note the offset at 10 and 20 seconds on the signal $x_2(t)$

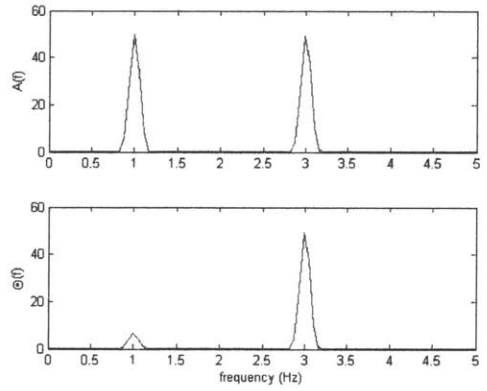

Figure A-2: $A(f)$ (upper) and $\Theta(f)$ (lower).

Appendix B

Motion Detection

A block diagram of the monitoring system is illustrated in figure B-1. The functions and interactions of each block are as follows:

1. The Hermes server, FTP server (Windows XP) and the cameras are connected on the same network with unique IP addresses for each.

2. Each camera FTP's JPEG images at 1 second intervals onto the FTP server in specified folders. Each folder is unique for each camera.

3. To start recording, Hermes server writes a file to the FTP server to start recording on a specific camera.

4. Matlab, in the FTP server, looks at the specified camera folder for JPEG images. Matlab then loads successive images and computes motion index M_n (equation 2.8) starting at a specified time. If there are no images or images are not uploaded for 60 seconds (default) or any time length, Matlab sends a command to the power control module to reboot the camera. If absence of images persists after a specified time, Matlab emails an error message. If recording is not started or stopped by Hermes on a specific camera, Matlab will keep deleting the JPEG files on the camera folder.

5. Matlab saves the motion indices M_n in a file (name.motion) and the corresponding JPEG filenames in a separate file (name.image) every 10 minutes (default)

or any time length. The files are named sequentially. JPEG, name.motion and name.image files can either be sent to the Hermes server or saved in a local directory.

6. To stop recording, Hermes server writes a file to the FTP server to stop recording on a specific camera.

7. Matlab stops recording at a specific time and the cycle can repeat.

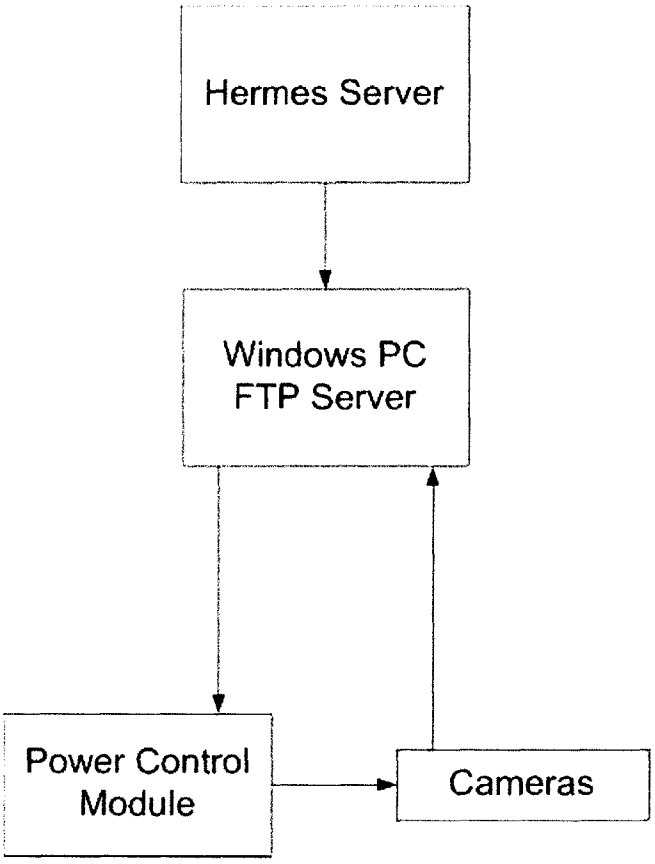

Figure B-1: Block diagram.

Appendix C

Hermes Identification Numbers

Mouse	Hermes ID		Mouse	Hermes ID
DKO	9050040505		Normal	5463040105
DKO 1	0920122903		Normal 1	9399111603
DKO 2	0921122903		Normal 2	9907120503
DKO 3	0922122903		Normal 3	9908120503
DKO 4	0902122703		Normal 4	9909120503
DKO 5	4630040604			
DKO 6	**3222031004**			

Bibliography

[1] Task Force of the European Society of Cardiology and the North American Society of Pacing and Electrophysiology. Heart rate variability: standards of measurements, physiological interpretation, and clinical use. Circulation 1996; 93:1043–1065.

[2] Klieger RE, Miller JP, Bigger Jr. JT, et al. Decreased Heart Rate Variability and Its Association with Increased Mortality After Acute Myocardial Infarction. Am J Cardiol 1987;59:256–262.

[3] Braun A, Trigatti B, Post M, Sato K, Simons M, Edelberg M, Rosenberg R, Schrenzel M, Krieger M. Loss of SR-BI Expression Leads to the Early Onset of Occlusive Atherosclerotic Coronary Heart Disease, Spontaneous Myocardial Infarctions, Severe Cardiac Dysfunction, and Premature Death in Apolipoprotein E-Deficient Mice. American Heart Assoc Circulation Research 2002;90:271–275.

[4] Gerhmann J, Hammer P, Maguire C, Wakimoto H, Triedman J, Berul C. Phenotypic screening for heart rate variability in the mouse. Am J Physiol Heart Circ Physiol 2000;279:H733–H740.

[5] Oefinger M. System for Remote Multichannel real-Time Monitoring of Mouse ECG via the Internet. Master's thesis, Massachusetts Institute of Technology, 2003.

[6] Acton S, Rigotti A, Landschulz K, Xu S, Krieger HHM. Identification of Scavenger Receptor SR-BI as a High Density Lipoprotein Receptor. Science 1996; 271:518–520.

[7] Carpeggiani C, L'Abbate A, Landi P, Michelassi C, Raciti M, Macerata A, Emdin M. Early assessment of heart rate variability is predictive of in-hospital death and major complications after acute myocardial infarction. International Journal of Cardiology 2004;96:361–368.

[8] Guyton AC, Hall JE. Textbook of Medical Physiology. W.B. Saunders Company, 2001.

[9] Dubin D. Rapid Interpretation of EKG's. Cover Publishing Company, 1994.

[10] Mark RG. Clinical Electrocardiography and Arrhythmias. Lecture Notes, 2004.

[11] McCance KL, Huether SE. Pathophysiology. The Biologic Basis for Disease in Adults and Children. Mosby, Inc, 2002.

[12] Akselrod A, Gordon D, Ubel FA, Shannon DC, Barger AC, Cohen RJ. Power spectrum analysis of heart rate fluctuations: a quantitative probe of beat-to-beat cardiovascular control. Science 1981;213:220–222.

[13] Clifford GD. Signal Processing Methods For Heart Rate Variability. Ph.D. thesis, Oxford University, 2002.

[14] Eckberg D. Sympathovagal Balance. Circulation 1997;96:3224–3232.

[15] Ryan C, Hollenberg M, Harvey DB, Gwynn R. Impaired parasympathethic responses after myocardial infarction. Am J Cardiol 1976;37:1013–1018.

[16] Wolf MW, Varigos GA, Hunt D. Sinus arrhythmia in acute myocardial infarction. Med J Aust 1978;2:52–53.

[17] Bigger Jr. JT, Fleiss JL, Steinman RC, Rolnitzky LM, Klieger RE, Rottman JN. Frequency Domain Measures of Heart Period Variability and Mortality after Myocardial Infarction. Circulation 1992;85:164 171.

[18] Singh N, Mironov D, Armstrong P, Ross A, Langer A. Heart Rate Variability Assessment Early After Myocardial Infarction. Circulation 1996;93:1388 1395.

[19] Janssen B, Leenders P, Smits J. Short-term and long-term blood pressure and heart rate variability in the mouse. Am J Physiol Regulatory Integrative Comp Physiol 2000;278:R215–R225.

[20] Hedman AE, Tahvanainen KU, Hartikainen JE, Hakumaki MO. Effect of sympathetic modulation and sympathovagal interaction on heart rate variability in anaesthetized dogs. Acta Physiol Scand 1995;155:205–214.

[21] Pan J, Tompkins W. A Real-Time QRS Detection Algorithm. IEEE Transactions on Biomedical Engineering 1985;32:230–236.

[22] Moody G, Mark RG, Zoccola A, Mantero S. Derivation of Respiratory Signals from Multi-lead ECGs. Computers in Cardiology 1985;12:113–116.

[23] Thomas RJ, Mietus JE, Peng CK, Goldberger AL. An ECG-Based Technique to Assess Cardiopulmonary Coupling during Sleep., Sleep In Press.

[24] Zong W, Moody GB, Jiang D. A Robust Open-source Algorithm to Detect Onset and Duration of QRS Complexes. Computers in Cardiology 1998;.

[25] Mark RG, Moody GB. ECG ARRYTHMIA ANALYSIS: DESIGN AND EVALUATION STARTEGIES. Advances in Processing and Pattern Analysis of Biological Signals 1996;251–272.

[26] Clifford GD, McSharry PE, Tarassenko L. Characterizing Artefact in the Normal Human 24-Hour RR Time Series to Aid Identification and Artificial Replication of Circadian Variations in Human Beat to Beat Heart Rate using a Simple Threshold, Computers in Cardiology 2002.

[27] Mitra SK, Kaiser JF. HANDBOOK FOR DIGITAL SIGNAL PROCESSING. John Wiley and Sons, 1993.

[28] Leon-Garcia A. Probability and Random Processes for Electrical Engineering. Addison-Wesley, 1994.